Regular article PJ2010679

for ***a special issue of Polymer Journal*** *entitled "Innovation of Concepts in Polymer Science, Japan"*

Running head:

Miscible Blend Dynamics

Dynamics in Miscible Blends of Polyisoprene and Poly(*p*-*tert*-butyl styrene) : Thermo-Rheological Behavior of Components

Quan Chen, Yumi Matsumiya, Keisuke Hiramoto, and Hiroshi Watanabe*

Institute for Chemical Research, Kyoto University, Uji, Kyoto 611-0011, Japan

*: to whom correspondence should be addressed.

Abstract

For miscible blends of moderately entangled *cis*-polyisoprene (PI) and poly(*p-tert*-butyl styrene) (PtBS), viscoelastic and dielectric properties were examined over a wide range of temperature T to discuss the thermo-rheological behavior of respective components. Because PI has the type-A dipole, whereas PtBS does not, the slow dielectric response of the blends was exclusively attributed to the global motion of the PI chains therein. In most of the blends examined, the viscoelastic relaxation was much slower than the dielectric relaxation, and PI and PtBS behaved as the fast and much slower components, respectively. In those blends, the PI relaxation was thermo-rheologically complex because the slow PtBS chains quenched the dynamic frictional heterogeneity in the time scale of the PI relaxation. In contrast, the viscoelastic response of PtBS was thermo-rheologically simple because the fast PI chains smeared the heterogeneity for PtBS. Nevertheless, PtBS exhibited no ordinary relaxation associated with the entanglement plateau but did exhibit Rouse-like relaxation slower than the entanglement-free Rouse process. This slow Rouse-like relaxation was attributed to the *pseudo-constraint release* mechanism for the PtBS chains activated by the global motion of the PI chains. A simple model based on this molecular picture described the G^* data of the blends well.

Key Words: *cis*-polyisoprene/poly(*p-tert*-butyl styrene) miscible blend, frictional heterogeneity, thermo-rheological complexity, entanglement, pseudo-constraint release

1. INTRODUCTION

In general, chemically different polymer chains are immiscible with each other because their mixing entropy is very small (practically zero). However, a considerable number of polymer pairs, including the pair of *cis*-polyisoprene (PI) and poly (vinyl ethylene) (PVE), is known to be miscible over a wide range of temperature T. Extensive studies have been conducted for such miscible blends to examine the dynamics of *monomeric* segments being related to the glass transition.[1-15] Those studies revealed characteristic features of the miscible blends such as the broad (almost two-step) glass transition noted in thermal measurements, the broad modes of segmental motion detected with NMR, and the broad and thermo-rheologically complex relaxation processes observed with the dielectric/viscoelastic methods. These features are related to the self-concentration effect[16] and the local composition fluctuation.[17] The monomeric segments of a given component chain tend to be locally concentrated because of the chain connectivity. This self-concentration results in a difference of the local environments for the segments of respective components, thereby providing these components with different effective glass transition temperatures, T_g^{eff}. The broad glass transition behavior, the broad motional modes, and the thermo-rheological complexity mentioned above are naturally related to this difference in T_g^{eff}. In addition, the local chemical composition fluctuates with time, which further broadens the motional modes of the segments to enhance the complexity.

Global chain dynamics in a length scale being comparable to the chain dimension is often affected by entanglement. The global chain dynamics in miscible blends is also a subject of interest. However, only a few studies have been conducted for the global dynamics and the entanglement effect.[18-23] Thus, blends of PI and poly(*p-tert*-butyl styrene) (PtBS) were chosen as model systems to examine the global dynamics of the components therein.[24-27] PI has the type-A dipole parallel along the chain backbone and its global motion activates slow dielectric relaxation,[28,29] whereas PtBS has no type-A dipole and is dielectrically inert in long time scales.[27] This difference between PI and PtBS enabled us to dielectrically examine, without any ambiguity, the global dynamics of PI in the blends. Furthermore, PI and PtBS have a negative interaction parameter and are miscible in a surprisingly wide range of T,[24,30] enabling a thorough test of the thermo-rheological behavior of the PI and PtBS chains in the miscible blends. This test revealed several characteristic features of the component dynamics, as explained below.

The dielectrically detected global dynamics of the PI chains in the blend is thermo-rheologically complex given that the PtBS motion is *much slower* than the PI motion to effectively quench the

fluctuation of local friction (determined by the local composition) in the time scale of the global PI relaxation and that the PI chain dimension is comparable to/smaller than the characteristic length of this frictional heterogeneity.[24-26] Furthermore, the dielectric data were subjected to the Williams-Landel-Ferry (WLF) analysis to determine a reference state in which the Rouse segment of PI in the blends had the same relaxation time τ_s as that in the bulk PI system.[26] The Rouse segment is the smallest motional unit for the global relaxation process and *not* identical to the monomeric segment governing the glass transition.[31-34] The analysis showed that the PI relaxation was slower in the blends, by a factor of 2-3, than in the iso-τ_s bulk possibly because of a topological constraint from the slow PtBS chains.[26] In addition, the entanglement length a in the blends was found to be well described by a simple mixing rule based on the number fraction n of the Kuhn segments of PI and PtBS:[27]

$$a = n_{PI} a_{PI}^{bulk} + n_{PtBS} a_{PtBS}^{bulk} \quad (1a)$$

with

$$a_{PtBS}^{bulk} = 11.7 \text{ nm}, \quad a_{PI}^{bulk} = 5.8 \text{ nm} \quad (1b)^{[35-37]}$$

This rule, differing from mixing rules assumed in literature,[20,23] is consistent with the current molecular picture that relates the entanglement density to the packing length.[35-37]

The previous study also examined the global dynamics of the PtBS chains entangled with the PI chains.[24,26] For this purpose, the complex modulus G_{PtBS}^* of the PtBS chains was estimated by subtracting the PI modulus G_{PI}^* (expressed in terms of the bulk PI modulus) from the blend modulus.[24,26] The G_{PtBS}^* data thus obtained were found to be thermo-rheologically simple given that the PI chains relaxed much faster than the PtBS chains thereby smearing the local frictional heterogeneity in the time scale of the PtBS relaxation and allowing the PtBS chain to relax through the same mechanism in the entire range of T.[24,26] Furthermore, the G_{PtBS}^* data were subjected to the WLF analysis to determine the iso-τ_s state for the Rouse segment of PtBS defined with respect to bulk PtBS. Comparison of the PtBS relaxation behavior in this iso-τ_s state revealed that the PtBS relaxation is slower in the blends, by a factor > 5, than in the bulk.[26] This large difference suggested that the PtBS chains in the blends relax through a *pseudo-constraint release* (*pseudo-CR*) mechanism activated by the global motion of PI chains entangling with (or *stitching*) the PtBS chains.[24,26]

It should be emphasized that the above features of the PI dynamics, the thermo-rheological complexity and the moderate retardation of the relaxation due to the constraint from PtBS, were

resolved, with no ambiguity, from the dielectric data exclusively detecting the global PI motion. In contrast, the PtBS dynamics was examined for the PtBS modulus, G_{PtBS}*, obtained after the subtraction of the estimated PI modulus in the blends, G_{PI}*. One might suspect that a small uncertainty in the estimated G_{PI}* resulted in some uncertainty in G_{PtBS}*. In addition, the subtraction based on the entanglement concept is valid only in a range of frequencies where the PI and PtBS chains have been cooperatively Rouse-equilibrated within the entanglement length, as revealed in recent work.[27]

Thus, for completeness, the PtBS dynamics was examined for model PI/PtBS blends having G_{PtBS}* >> G_{PI}* (having the PI relaxation time τ_{PI} much shorter than τ_{blend} of the blend) in the entire range of T. For these blends, small numerical uncertainties in G_{PI}* hardly affected the G_{PtBS}* values. It turned out that those model blends unequivocally exhibit the features explained above, the thermo-rheological simplicity and the strong retardation of the PtBS relaxation due to the entangling PI chains that activate the pseudo-CR mechanism. The behavior of the other type of blend having G_{PtBS}* ~ G_{PI}* (having τ_{PI} ~ τ_{blend}) was also examined to discuss the entanglement relaxation and pseudo-CR processes of the PI and PtBS chains therein. Details of the results are presented in this paper.

2. EXPERIMENTAL

2.1 Materials

Table 1 shows a list of PI and PtBS samples utilized in this study (and a previous study[38] relevant to this study). An oligomeric PI sample, PI3, was anionically synthesized at 30˚C in vacuo, with benzene and *sec*-butyllithium being utilized as the solvent and initiator, respectively. The other PI and PtBS samples were anionically synthesized in the previous studies,[24,27,38] except the commercially supplied PI20 sample (from Kuraray Co).[24] The PI3 sample was characterized with GPC (Co-8020 and DP-8020, Tosoh) having a refractive index (RI) monitor (LS-8000, Tosoh Co) and also with ^{1}H-NMR (MERCURYplus AS400, Varian) for the chain end/microstructure analysis. The characteristics of this sample are summarized in Table 1 together with those of the previous samples. The microstructure of the PI3, PI53, PI99 samples was the same within experimental resolution, 1,4-*cis* : 1,4-*trans* : 3,4 = 79 : 14 : 7. This microstructure, indistinguishable from that of

the PI20 sample,[26] allowed all PI/PtBS blends to be in the miscible state in the entire range of T examined ($T \leq 90^{\circ}$C).

The materials subjected to viscoelastic and dielectric measurements were the PI20/PtBS42, PI20/PtBS70, and PI99/PtBS42 blends. The PI and PtBS chains therein were entangled with each other, as judged from Eq. 1. A PI3/PtBS42 blend containing oligomeric PI3 was also examined as an entanglement-free, reference system. These blends were prepared with the method described previously:[26,30] Prescribed masses of the PtBS and PI samples were dissolved in tetrahydrofuran (THF) at a total concentration of 10 wt% and then precipitated in a dropwise manner into an excess methanol/acetone (8/2 wt/wt) mixture vigorously stirred by a magnetic bar. The blends were recovered *via* decantation and thoroughly dried under vacuum first at room temperature and then at 120 °C. The blends thus prepared were transparent, which is in accord with the PI/PtBS miscibility.

2.1 Measurements

Linear viscoelastic and dielectric measurements were conducted for the entangled PI20/PtBS42, PI20/PtBS70, and PI99/PtBS42 blends all having the same PI content, w_{PI} = 55.7 wt% (PI volume fraction ϕ_{PI} = 0.59; evaluated under the assumption of volume additivity). The measurements were made also for the PI and PtBS components in respective bulk states, and the data are summarized in the Appendix. For comparison, the viscoelastic behavior was examined also for the entanglement-free PI3/PtBS42 reference blend (w_{PI} = 55.7 wt%).

The viscoelastic measurements were conducted with a laboratory rheometer (ARES, TA Instruments) at several temperatures $T \leq 90^{\circ}$C. A parallel plate fixture with a diameter of 8 mm was utilized. The oscillatory strain amplitude was kept small ($\gamma_0 \leq 0.1$) to ensure the linearity of the storage and loss moduli, G' and G''.

The dielectric measurements were conducted at $T \leq 90^{\circ}$C with an impedance analyzer/dielectric interface system (1260 and 1296, Solartron). The samples were charged in a dielectric cell composed of parallel electrodes and a guard electrode. The dielectric data were summarized as plots against the angular frequency, $\omega = 2\pi f$ with f being the frequency in Hz.

3. RESULTS AND DISCUSSION

3.1 Overview of dynamic behavior of blends with $\tau_G >> \tau_\varepsilon$

Figure 1 compares the data of the storage and loss moduli, $G'(\omega)$ and $G''(\omega)$, the dielectric loss, $\varepsilon''(\omega)$, and the decrease of dynamic dielectric constant from its static value, $\Delta\varepsilon'(\omega) = \varepsilon'(0) - \varepsilon'(\omega)$, measured for the PI20/PtBS42 and PI20/PtBS70 blends having the same w_{PI} (= 55.7 wt%) and the same M_{PI} but different M_{PtBS}. These data are double-logarithmically plotted against the angular frequency, ω, and the comparison is made at the lowest and highest temperatures examined, T = 20 and 90 ˚C. The $\Delta\varepsilon'(\omega)$ and ε'' data, multiplied by a factor of 10^3, are shown in a range of ω where the direct current contribution due to ionic impurities contributed negligibly to the data. These data exclusively detect the global motion (end-to-end vector fluctuation) of the PI component chains in the blends. (The PtBS chains have no type-A dipole and are dielectrically inert at the frequencies examined.[27])

The PtBS chains in those blends have the molecular weight M_{PtBS} comparable to the entanglement molecular weight of bulk PtBS, $M_{e,PtBS}^{bulk} = 37.6\times10^3$,[37] and are barely entangled in the bulk. Nevertheless, the entanglement length a changes upon blending,[27] and the corresponding $M_{e,PtBS}$ and $M_{e,PI}$ in the blends are evaluated from Eq. 1 as:

$$M_{e,PtBS} = 10.5\times10^3,\ M_{e,PI} = 5.7\times10^3 \qquad (2)$$

(The a_{PtBS}^{bulk} and a_{PI}^{bulk} values given by Eq. 1b, the molecular weights of the Kuhn segments, $M_{K,PI}$ = 130 and $M_{K,PtBS}$ = 1500,[26,37] and the $M_{e,PtBS}^{bulk}$ and $M_{e,PI}^{bulk}$ $(= 5.0\times10^3)$[37] value were utilized to obtain the M_e values in Eq. 2.) M_{PtBS} and M_{PI} of the PI and PtBS chains are larger than these $M_{e,PtBS}$ and $M_{e,PtBS}$ by a factor of ≅ 4 or more, indicating that the PtBS chains in the blends are moderately entangled with the coexisting PI chains. In Figure 1, the horizontal dashed lines indicate the entanglement plateau modulus corresponding to the M_e values given in Eq. 2:

$$G_N = \left\{\frac{C_{PI}}{M_{e,PI}} + \frac{C_{PtBS}}{M_{e,PtBS}}\right\}RT \qquad (3)$$

C_{PI} and C_{PtBS} represent the mass concentration of PI and PtBS in the blends, respectively, R is the gas constant, and T is the absolute temperature. At low T, the storage modulus G' does not show a plateau at this G_N but exhibits a power-law behavior together with the loss modulus, $G' \cong G'' \propto \omega^{\beta}$ with $\beta \cong 1/2$, and the moduli in this power-law zone are insensitive to M_{PtBS}; see the top panel of Figure 1. These features reflect the cooperative Rouse equilibration of the PI and PtBS chains within the entanglement length,[27] as explained later in more detail. Note also that the equilibration

process itself hardly activates a change of the end-to-end vector of the PI chain and is dielectrically inert.

The blends exhibit the terminal viscoelastic and dielectric relaxation characterized by the low-ω asymptotes[28,29] of $G'(\propto \omega^2)$, $G''(\propto \omega)$, $\Delta\varepsilon'(\propto \omega^2)$, and $\varepsilon''(\propto \omega)$. (The expression of $\Delta\varepsilon'(\omega)$ and $\varepsilon''(\omega)$ in terms of the relaxation spectrum is formally identical to that of $G'(\omega)$ and $G''(\omega)$, and thus $\Delta\varepsilon'(\omega)$ and $\varepsilon''(\omega)$ exhibit the low-ω asymptotes similar to those of $G'(\omega)$ and $G''(\omega)$.[28,29]) The terminal viscoelastic and dielectric relaxation times, τ_G and τ_ε, are evaluated from these asymptotes:[28,29]

$$\tau_G = \left[\frac{G'}{\omega G''}\right]_{\omega\to 0}, \quad \tau_\varepsilon = \left[\frac{\Delta\varepsilon'}{\omega\varepsilon''}\right]_{\omega\to 0} \tag{4}$$

In Figure 1, the thick arrows indicate the terminal viscoelastic relaxation frequency, $\omega_G = 1/\tau_G$. The terminal dielectric relaxation frequency, $\omega_\varepsilon = 1/\tau_\varepsilon$, was very close to a frequency ω_x where the $\Delta\varepsilon'$ and ε'' curves cross each other. Clearly, ω_G is much smaller than ω_x (= ω_ε). This fact indicates that the PI and PtBS chains are the fast and *much* slower components, respectively, in the PI20/PtBS42 and PI20/PtBS70 blends and that the terminal viscoelastic relaxation of the blends is dominated by the PtBS chains.

This PtBS dominance can be also examined straightforwardly with the aid of a blending rule for the complex modulus G^* (= $G'+iG''$) and the relaxation modulus $G(t)$ valid in the entanglement relaxation regime after completion of the Rouse equilibration within the entanglement length:[25-27]

$$G_{\text{blend}}^*(\omega) = G_{\text{PI,e}}^{\text{bld}}*(\omega) + G_{\text{PtBS}}^{\text{bld}}*(\omega) \tag{5a}$$

$$G_{\text{blend}}(t) = G_{\text{PI,e}}^{\text{bld}}(t) + G_{\text{PtBS}}^{\text{bld}}(t) \tag{5b}$$

with

$$G_{\text{PI,e}}^{\text{bld}}*(\omega) = \phi_{\text{PI}} I_{\text{PI}} \{\upsilon_{\text{maj}} G_{\text{PI}}^{\text{bulk}}*(\omega\lambda_{\text{PI}}^{\text{maj}} Q_{\text{maj}}^{2.33}) + \upsilon_{\text{min}} G_{\text{PI}}^{\text{bulk}}*(\omega\lambda_{\text{PI}}^{\text{min}} Q_{\text{min}}^{2.33})\} \tag{6a}$$

$$G_{\text{PI,e}}^{\text{bld}}(t) = \phi_{\text{PI}} I_{\text{PI}} \{\upsilon_{\text{maj}} G_{\text{PI}}^{\text{bulk}}(t/\lambda_{\text{PI}}^{\text{maj}} Q_{\text{maj}}^{2.33}) + \upsilon_{\text{min}} G_{\text{PI}}^{\text{bulk}}(t/\lambda_{\text{PI}}^{\text{min}} Q_{\text{min}}^{2.33})\} \tag{6b}$$

Equation 5 merely indicates the additivity of moduli of the PI chains ($G_{\text{PI,e}}^{\text{bld}}*(\omega)$, $G_{\text{PI,e}}^{\text{bld}}(t)$) and the PtBS chains ($G_{\text{PtBS}}^{\text{bld}}*(\omega)$, $G_{\text{PtBS}}^{\text{bld}}(t)$) in the blends; that is, the stress additivity. $G_{\text{PI,e}}^{\text{bld}}*(\omega)$ and $G_{\text{PI,e}}^{\text{bld}}(t)$ are the moduli for the entanglement relaxation of PI and include no contribution from the Rouse equilibration. In Eq. 6, these moduli are approximated to have the same mode distribution as

in bulk and expressed in terms of the moduli data of bulk PI at the same T, $G_{\rm PI}^{\rm bulk}*(\omega)$ and $G_{\rm PI}^{\rm bulk}(t)$. This approximation is valid for the terminal relaxation of the fast component in the blends, as noted from extensive data for entangled PI/PI blends.[28,39-41] (Note that the moduli data of bulk PI contain a contribution from the Rouse equilibration completing at the time τ_a. However, this contribution becomes negligible at low ω and long t, in particular for the relaxation modulus $G_{\rm PI}^{\rm bulk}(t)$ at long t because a modulus ratio for the Rouse equilibration and the entanglement relaxation rapidly decays with t as $\exp\left\{-t(\tau_a^{-1}-\tau_{\rm ent}^{-1})\right\}$ ($\tau_{\rm ent}$ = entanglement relaxation time) and vanishes in the time scale of $t \sim \tau_{\rm ent}$.)

More comments need to be made for Eq. 6. The dielectric mode distribution of the PI20 chains in the blend at low T is broader than that in bulk, as most clearly noted later in Figure 2. This fact indicates that the chains are classified into the minority and majority having different relaxation times. Namely, at low T, the PtBS motion is much slower than the PI motion to quench the dynamic frictional heterogeneity during the terminal relaxation process of PI.[26] Then, some PI chains (albeit a minority) in a PtBS-rich region feel the friction larger than that for the remaining PI chains (the majority).[26] In Eq. 6, this feature was considered to express $G_{\rm PI,e}^{\rm bld}*(\omega)$ and $G_{\rm PI,e}^{\rm bld}(t)$ as a sum of the contributions from the majority and minority having the fractions $\upsilon_{\rm maj}$ and $\upsilon_{\rm min}$.

The factors $I_{\rm PI}$ and $\lambda_{\rm PI}$ appearing in Eq. 6 represent corrections for the changes of the entanglement length a and dielectric relaxation time of PI, $\tau_\varepsilon^{\rm PI}$, upon blending:[27]

$$I_{\rm PI} \equiv \left(\frac{a_{\rm PI}^{\rm bulk}}{a}\right)^2 , \quad \lambda_{\rm PI} = \frac{\tau_\varepsilon^{\rm PI\ in\ blend}}{\tau_\varepsilon^{\rm bulk\ PI}} \tag{7}$$

$I_{\rm PI}$ is evaluated with the aid of Eq. 1. The $\lambda_{\rm PI}$ factor, separately defined for the majority and minority PI, is obtained from the dielectric $\tau_\varepsilon^{\rm PI}$ data of PI in the blend and bulk.[26] The Q factor appearing in Eq. 6 represents a change of the PI dynamics upon blending; more specifically, a change of the contribution of the dynamic tube dilation/constraint release (DTD/CR) mechanisms to the relaxation of entangled PI.[26] The Q factor is evaluated from the τ_ε and $\tau_{\rm G}$ data of the blend and bulk PI with the aid of the empirical Eq. 9 of Ref. 26, with the numerical coefficients therein given by (B, α, q) = (0.35, 0.2, 2.5) for the blends with $\phi_{\rm PtBS}$ = 0.41 (=ϕ_2 in Eq. 9 of Ref. 26). For those blends, Q for the majority PI decreased only moderately, from 1.2 to 1, on the increase of T from 20°C to 90°C, and the $Q^{2.33}$ factor appearing in Eq. 6 gave a minor correction for the $\tau_\varepsilon^{\rm PI\ in\ blend}/\tau_\varepsilon^{\rm bulk\ PI}$ ratio.

Figure 2 compares the $G_{\text{blend}}^*(\omega)$ data of the PI20/PtBS42 blend (squares) and the modulus $G_{\text{PI,e}}^{\text{bld}}*(\omega)$ for the entanglement relaxation of PI20 therein (thick solid curves) estimated from the $G_{\text{PI}}^{\text{bulk}}*(\omega)$ data; cf. Eq. 6a. The triangles show the dielectric ε'' data of the blend multiplied by a factor of 10^4. Figure 3 shows the results of the corresponding comparison of the relaxation moduli, $G_{\text{blend}}(t)$ and $G_{\text{PI,e}}^{\text{bld}}(t)$ converted from the $G_{\text{blend}}^*(\omega)$ and $G_{\text{PI}}^{\text{bulk}}*(\omega)$ data with the previously reported iteration method.[42] The triangles show the dielectric relaxation function $\varepsilon(t)$ of the blend converted from the ε'' data.

For the estimation of $G_{\text{PI,e}}^{\text{bld}}*(\omega)$, the ε'' data of the blend were fitted with the $\varepsilon_{\text{bulk PI}}''$ data of bulk PI multiplied by the PI volume fraction in the blend, $\phi_{\text{PI}} = 0.59$. At low T (20˚C), the dielectric mode distribution of the blend was broader than that of bulk PI because of the quenched frictional heterogeneity for PI in the blend explained earlier; see the triangles in the top panel of Figure 2. Thus, the dielectric contributions from the majority and minority PI in the blend were separately considered and expressed in terms of the $\varepsilon_{\text{bulk PI}}''$ data as $\phi_{\text{PI}}\upsilon_{\text{maj}}\varepsilon_{\text{bulk PI}}''(\omega\lambda_{\text{PI}}^{\text{maj}})$ and $\phi_{\text{PI}}\upsilon_{\text{min}}\varepsilon_{\text{bulk PI}}''(\omega\lambda_{\text{PI}}^{\text{min}})$, with λ_{PI} representing a ω-shift from the bulk data, and the ε'' data of the blend were fit with a sum of these contributions. The fitting was well achieved, as shown by the thin solid curve in the top panel of Figure 2, where the contributions from the majority and minority PI (with $\upsilon_{\text{maj}} = 0.7$ and $\upsilon_{\text{min}} = 0.3$) are shown with the thin dotted curves. (The corresponding dielectric relaxation functions of the majority and minority are shown with the dotted curves in the top panel of Figure 3.) In contrast, at high T (90˚C), the dielectric mode distribution of the blend was very close to that of bulk PI, and the ε'' data were satisfactorily fitted by $\phi_{\text{PI}}\varepsilon_{\text{bulk PI}}''(\omega\lambda_{\text{PI}}^{\text{maj}})$ ($\upsilon_{\text{maj}} = 1$, $\upsilon_{\text{min}} = 0$), as shown with the thin solid curve in the bottom panel of Figure 2. The complex modulus $G_{\text{PI,e}}^{\text{bld}}*(\omega)$ shown in Figure 2 was estimated from these υ values and the λ_{PI} values with the aid of Eq. 6. The entanglement relaxation modulus of PI, $G_{\text{PI,e}}^{\text{bld}}(t)$ shown in Figure 3, was converted from this $G_{\text{PI,e}}^{\text{bld}}*(\omega)$.

As noted in Figure 2, $G_{\text{PI,e}}^{\text{bld}}*(\omega)$ is much smaller than $G_{\text{blend}}^*(\omega)$ in the entire ranges of ω and T. Correspondingly, $G_{\text{PI,e}}^{\text{bld}}(t)$ is much smaller than $G_{\text{blend}}(t)$ at the t and T examined; cf. Figure 3. These results indicate that the PtBS chain dominates the terminal viscoelastic relaxation of the blend, which was the case also for the PI20/PtBS70 blend having larger M_{PtBS}. Thus, for the PI20/PtBS42 and PI20/PtBS70 blends, the PtBS moduli obtained by the subtraction, $G_{\text{PtBS}}^{\text{bld}}*(\omega) = G_{\text{blend}}*(\omega) - G_{\text{PI,e}}^{\text{bld}}*(\omega)$ and $G_{\text{PtBS}}^{\text{bld}}(t) = G_{\text{blend}}(t) - G_{\text{PI,e}}^{\text{bld}}(t)$, are practically indistinguishable from the $G_{\text{blend}}^*(\omega)$ and $G_{\text{blend}}(t)$ data and hardly contain numerical uncertainty due to the subtraction; see the small filled circles in Figures 2 and 3. These blends serve as the model systems that enable the

unambiguous test of the thermo-rheological behavior of the PtBS chain therein. This test is performed later for the moduli $G_{\mathrm{PtBS}}^{\mathrm{bld}}{}^{*}(\omega)$ and $G_{\mathrm{PtBS}}^{\mathrm{bld}}(t)$ evaluated in the ranges of ω and t where the PI and PtBS chains have been Rouse-equilibrated within the entanglement segment to exhibit $G'(\omega)$, $G(t) \leq G_{\mathrm{N}}$: The blending rule considering this segment as the basic unit for the chain motion, Eqs. 5 and 6, is valid at those ω and t.

Now, the Rouse-like power-law behavior seen at low T, $G' \cong G'' \propto \omega^{\beta}$ with $\beta \cong 1/2$, and the corresponding lack of the entanglement plateau at $G' = G_{\mathrm{N}}$ (cf. top panel of Figure 1) are analyzed. This plateau prevails only when the global chain motion is much slower than the Rouse equilibration within the entanglement length a. In the PI/PtBS blends at low T, the slow PtBS chains hinder the fast PI chain from exploring the local conformations at lengths $\leq a$ within its intrinsic Rouse equilibration time thereby retarding the equilibration of the PI chain.[27] If the time τ_a necessary for the cooperative Rouse equilibration of PI and PtBS is close to the terminal entanglement relaxation time of PI, the power-law behavior resulting from this equilibration masks the entanglement plateau. This molecular argument can be tested from a comparison of τ_a and the dielectric τ_ε of PI (cf. Eq.4), the former being evaluated from the continuous Rouse relationship:[27,43]

$$G'(1/\tau_a) = G''(1/\tau_a) = 1.111\left\{\frac{C_{\mathrm{PI}}}{M_{\mathrm{e,PI}}} + \frac{C_{\mathrm{PtBS}}}{M_{\mathrm{e,PtBS}}}\right\}RT \qquad (8)$$

In the top panel of Figure 1, the thin arrow shows the Rouse equilibration frequency $\omega_a = 1/\tau_a$ evaluated by applying Eq. 8 to the G^* data at 20˚C. The dielectric $\omega_\varepsilon = 1/\tau_\varepsilon$ of PI is very close to the frequency ω_{x} where the $\Delta\varepsilon'$ and ε'' curves cross each other, as explained earlier. Clearly, ω_a almost coincides with ω_{x} (= ω_ε). Thus, the PI20 chain in the PI20/PtBS42 and PI20/PtBS70 blends fully relaxes immediately after it is Rouse-equilibrated together with the PtBS chain, which confirms the above molecular argument. This fact becomes a key in our later discussion of the PtBS relaxation in the blend.

In relation to the above result, it should be noted that the Rouse equilibration is a local process occurring at length scales $\leq a$. Thus, the power-law behavior associating this process is expected to be insensitive to the component molecular weights M given that M is well above M_{e}. In fact, the G^* data in this power-law zone are indistinguishable for the PI20/PtBS42 and PI20/PtBS70 blends having different M_{PtBS}; see the top panel of Figure 1. Furthermore, the G^* data of the PI99/PtBS42 blend having different M_{PI} (shown later in Figure 4) were also close to those of the PI20/PtBS42 and PI20/PtBS70 blends in the power-law zone. These results are consistent with the above

expectation, lending support to the molecular picture of the retarded, cooperative Rouse equilibration of the PI and PtBS chains.

3.2 Overview of dynamic behavior of blends with $\tau_G \sim \tau_\varepsilon$

Figure 4 shows the G', G'', $\Delta\varepsilon'$, and ε'' data for the PI99/PtBS42 blend (w_{PI} = 55.7 wt%) at representative temperatures as indicated. (The $\Delta\varepsilon'$ and ε'' data are multiplied by a factor of 10^2.) The horizontal dashed line shows the entanglement plateau modulus G_N expected at 20˚C (cf. Eq. 3). The thick arrows indicate the viscoelastic relaxation frequency $\omega_G = 1/\tau_G$ (cf. Eq. 4) evaluated for the blend at respective temperatures, and the thin arrow shows the Rouse equilibration frequency $\omega_a = 1/\tau_a$ (cf. Eq.8) at 20˚C. The dielectric $\omega_\varepsilon = 1/\tau_\varepsilon$ of PI (with τ_ε being defined by Eq. 4) was close to the frequency ω_x where the $\Delta\varepsilon'$ and ε'' curves cross each other.

As noted in Figure 4, the power-law behavior due to the cooperative Rouse equilibration of PI and PtBS masks the entanglement plateau at 20˚C. This feature is similar to that seen in Figure 1 for the lower-M_{PI} PI20/PtBS42 and PI20/PtBS70 blends. In fact, the G^* data of the PI99/PtBS42 blend in this power-law zone are close to those of the latter two blends. However, important differences are also noted. For the PI99/PtBS42 blend, ω_G is close to the dielectric ω_ε (= ω_x) even at the lowest T examined, 20˚C, and ω_ε is much lower than ω_a. The close coincidence of ω_G and ω_ε demonstrates a large contribution of the PI99 chains to the terminal viscoelastic relaxation of the blend, and the large separation between ω_ε and ω_a indicates that the PI99 chain exhibits the global relaxation well after its Rouse equilibration. A delicate hump of the G'' data at 20˚C, noted for the data points at ω = 0.3-0.03 s^{-1} that lie above the power-law line, reflects this separation. (No corresponding hump is seen for the data of the low-M_{PI} blends in the top panel of Figure 1.) These differences are naturally related to the high molecular weight of PI99 ($M_{PI99} \cong 5M_{PI20}$) that results in the global motion much slower for PI99 than for PI20.

The significance of the PI99 contribution to the terminal viscoelastic relaxation of the blend can be further examined with the aid of Eq. 6a. The modulus $G^{bld}_{PI,e}*$ for the entanglement relaxation of PI99, specified by Eq. 6a, was estimated from the τ_ε and τ_G data of the blend and bulk PI99 and the $G^{bulk}_{PI}*$ data of bulk PI99, as explained earlier for the low-M_{PI} blends. (For PI99, the minority content was negligibly small and $G^{bld}_{PI,e}*$ was estimated from Eq. 6a with υ_{min} = 0.) The $G^{bld}_{PI,e}*$ thus obtained are shown in Figure 4 with the thick solid curves. These curves are close to the $G_{blend}*$ data of the PI99/PtBS42 blend in particular at high T, confirming the significant PI99 contribution to the $G_{blend}*$ data in the terminal relaxation regime.

3.3 Thermo-rheological behavior of PI in blends

The dielectric $\Delta\varepsilon'$ and ε'' data of the PI/PtBS blends exclusively detect the global PI motion even for the case that the PI motion is much faster than the PtBS motion. (The Rouse equilibration within the entanglement length does not activate a change of the end-to-end vector except at the chain ends and hardly affects the dielectric data.) Thus, those data enable us to examine the thermo-rheological behavior of PI without any ambiguity over the entire range of T. The top and bottom panels of Figure 5, respectively, show the time-temperature superposition of the dielectric data of the PI20/PtBS42 and PI99/PtBS42 blends examined in this study. (The results for the PI20/PtBS70 blend were almost indistinguishable from those for the PI20/PtBS42 blend and are not shown here.) The reference temperature was chosen to be T_r = 90˚C. The $\Delta\varepsilon'$ and ε'' data at respective T are multiplied by the intensity factor $b_T = T/T_r$ (with T and T_r in K unit) and shifted along the ω axis to achieve the best superposition at ω higher than the ε''-peak frequency, ω_{peak}. For clarity of the plots, only the data at representative T are shown, and the $\Delta\varepsilon'$ data are multiplied by a factor of $10^{1.5}$. For comparison, the middle panel shows the shifted data (with T_r = 90˚C) for the previously examined PI53/PtBS42 blend[38] having the same w_{PI} (= 55.7 wt%) and the same M_{PtBS} (= 41.8×10^3). For respective blends, the solid curves show the dielectric data of the PI components in the bulk state at 90˚C. These bulk data are multiplied by the PI volume fraction in the blend, ϕ_{PI} = 0.59, and shifted along the ω axis to match ω_{peak} with the blend data.

As noted in Figure 5, the shift is fairly successful for the ε'' data (even at $\omega < \omega_{peak}$) while a non-negligible failure prevails for the $\Delta\varepsilon'$ data at $\omega < \omega_{peak}$ in particular for the PI20/PtBS42 and PI53/PtBS42 blends. (Because $\Delta\varepsilon'$ is much more sensitive to slow dielectric modes compared to ε'',[29] the failure of the superposition is more clearly resolved for $\Delta\varepsilon'$.) This failure is mostly related to the spatial frictional heterogeneity for the PI chains:[24,26] At sufficiently low T where the PtBS motion is much slower than the PI motion, this heterogeneity survives during the terminal relaxation process of PI so that some PI chains (minority) stay in a PtBS-rich region and feel the friction larger than that for the majority. This heterogeneity is smeared within a random coil of a high-M_{PI} chain having the end-to-end distance R_{PI} well above the correlation length of the heterogeneity. For this reason, the failure is less significant for the PI99 chain (bottom panel) than for the PI20 and PI53 chains (top and middle panels).

The shift factor $a_{T,\varepsilon}$ utilized for the superposition in Figure 5 represents changes of the dielectric relaxation time τ_ε of the majority PI with T.[26] The top panel of Figure 6 shows the $a_{T,\varepsilon}$

data for the PI/PtBS blends with w_{PI} = 55.7 wt% examined in this and previous[38] studies. These data were subjected to a minor correction for a change of the DTD/CR contribution[26] to the PI relaxation with T (as explained earlier for Eq.6) and then subjected to the standard WLF analysis. This analysis enabled us to determine the iso-τ_s temperatures $T_{iso\text{-}PI}$ where the Rouse segment of PI had the same relaxation time τ_s in the blend and bulk PI system. Specifically, $T_{iso\text{-}PI}$ for the PI chains in the blends that corresponds to T_{iso-PI}^{bulk} = 30˚C for bulk PI was found to be:

$$T_{iso\text{-}PI} = 60^{\circ}\text{C (for PI/PtBS blends with } w_{PI} = 55.7 \text{ wt\%}) \quad (9)$$

In the bottom panel of Figure 6, the shift factor $a_{T,iso\text{-}PI}$ re-evaluated for this $T_{iso\text{-}PI}$ is plotted against a temperature difference, $T-T_{iso\text{-}PI}$. These $a_{T,iso\text{-}PI}$ data are indistinguishable for the PI chains having the same w_{PI} but different M_{PI} (PI20, PI53, and PI99) and are excellently described by the WLF equation for bulk PI shown with the solid curve (cf. Appendix):

$$\log a_T = -\frac{4.425(T - T_{iso\text{-}PI})}{140.0 + T - T_{iso\text{-}PI}} \quad (\text{with } T_{iso-PI}^{bulk} = T_{r,bulk} = 30^{\circ}\text{C}) \quad (10)$$

The coincidence of $T_{iso\text{-}PI}$ for those PI chains demonstrates that τ_s in the blends is determined by the local chemical composition irrespective of M_{PI}.

Concerning this result, one might attempt to apply the self-concentration model[16] to an effective $T_{g,PI}^{eff}$ corresponding to this $T_{iso\text{-}PI}$ ($T_{g,PI}^{eff} = T_{g,PI}^{bulk} + T_{iso\text{-}PI} - T_{iso-PI}^{bulk}$) thereby estimating a local effective composition. However, this model was developed for the local concentration of *monomeric* segments while the iso-τ_s temperatures $T_{iso\text{-}PI}$ is defined for the *Rouse* segments, the latter being the smallest motional unit for the rubbery relaxation. These two types of segments are not identical to each other and exhibit different T dependence of the friction coefficient at low T (~ T_g), as is well known from the fact[31-33] that the G^* data of homopolymers at low T and high ω are thermo-rheologically complex and associated with complicated changes of the rheo-optical data. Thus, the self-concentration model should not be utilized in the analysis of $T_{iso\text{-}PI}$.

3.4 Thermo-rheological behavior and relaxation mechanism of PtBS in blends with $\tau_G >> \tau_\varepsilon$

In the high-M_{PI} PI99/PtBS42 blend, the modulus $G_{PI,e}^{bld}$* for the entanglement relaxation of PI is close to the G_{blend}* data at low ω (in particular at $T \geq 50^{\circ}$C; see Figure 4) so that the PtBS modulus therein, G_{PtBS}^{bld}* = G_{blend}* – $G_{PI,e}^{bld}$* (cf. Eq. 5a), cannot be evaluated with sufficient numerical accuracy. However, for the low-M_{PI} PI20/PtBS42 and PI20/PtBS70 blends having G_{blend}* >>

$G^{\rm bld}_{\rm PI,e}$*, $G^{\rm bld}_{\rm PtBS}$*(ω) and $G^{\rm bld}_{\rm PtBS}(t)$ were evaluated with negligibly small uncertainty and practically coincided with the $G_{\rm blend}$*(ω) and $G_{\rm blend}(t)$ data; see Figures 2 and 3. Thus, this section utilizes the PtBS moduli $G^{\rm bld}_{\rm PtBS}$*(ω) and $G^{\rm bld}_{\rm PtBS}(t)$ in those low-$M_{\rm PI}$ blends to test the thermo-rheological behavior and the relaxation mechanism of the PtBS chains therein.

For convenience of this test, the PI3/PtBS42 blend ($w_{\rm PI}$ = 55.7 wt%) containing the oligomeric PI3 was chosen as the reference system. In this blend, the PtBS42 chains are not entangled among themselves because the molecular weight $M_{\rm PtBS42}$ of these chains is well below the entanglement molecular weight in a PtBS solution with $\phi_{\rm PtPS}$ = 0.41 (corresponding to $w_{\rm PtBS}$ = 44.3 wt% in the blend):

$$M^{\rm soln}_{\rm e,PtBS} = M^{\rm bulk}_{\rm e,PtBS}/\phi^{1.3}_{\rm PtBS} = 1.2\times10^5 \qquad (11)$$

Furthermore, the oligomeric PI3 has $M_{\rm PI3} < M_{\rm e,PI}$ (= 5.7×10^3 in the blend; cf. Eq. 2) and exhibits neither PI-PI nor PI-PtBS entanglement. Thus, the PI3/PtBS42 blend serves as the reference system showing the *intrinsic* entanglement-free relaxation behavior of the PtBS42 chain affected only by the relaxation time $\tau_{\rm s}$ of the Rouse segment of PtBS. The G* data of this blend obeyed the time-temperature superposition at T/°C = 20-80 and ω/s^{-1} = 10^{-2}-10^2 because the oligomeric PI3 relaxed much faster than PtBS42 and negligibly contributed to the data. These G* data, reduced at $T_{\rm r}$ = 20°C, are shown in Figure 7, and the corresponding shift factor $a_{\rm T,G}$ is shown later in Figure 10. The G* data exhibit the Rouse-like ω dependence, as expected for the non-entangled PtBS42 chain. These data serve as the reference data for the PtBS42 and PtBS70 chains in the non-entangled state, as explained later in more detail.

For the PI20/PtBS42 and PI20/PtBS70 blends ($w_{\rm PI}$ = 55.7 wt%), the moduli $G^{\rm bld}_{\rm PtBS}$*(ω) and $G^{\rm bld}_{\rm PtBS}(t)$ of the PtBS chains were evaluated in the range of ω and t where the $G'(\omega)$ and $G(t)$ data of the blends were below $G_{\rm N}$ and Eq. 6 based on the entanglement concept is valid; cf. Figures 2 and 3. In Figure 8, the modulus $G^{\rm bld}_{\rm PtBS}$*(ω) is reduced by the intensity factor $b_{\rm T}$ = $T/T_{\rm r}$ with $T_{\rm r}$ = 293 K (20°C) and shifted along the ω axis to make the best superposition. The corresponding shift of $G^{\rm bld}_{\rm PtBS}(t)$ is made in Figure 9. Good superposition is seen for $G^{\rm bld}_{\rm PtBS}$*(ω) and $G^{\rm bld}_{\rm PtBS}(t)$, in particular for the latter. (Note that a contribution of the Rouse equilibration within the entanglement length to the relaxation modulus $G^{\rm bld}_{\rm PtBS}(t)$, *even if it remains at short t*, decays rapidly as $\exp\left\{-t(\tau_a^{-1}-\tau_{\rm ent}^{-1})\right\}$ and completely vanishes in the time scale of entanglement relaxation, $t \sim \tau_{\rm ent}$.)

The above results allow us to conclude the thermo-rheological simplicity of the PtBS dynamics in those blends. This simplicity prevailed because the PI20 chain therein relaxed much faster than

the PtBS chains (cf. Figure 1) thereby allowing the PtBS relaxation mechanism to remain the same in the entire range of T. (In relation to this point, it should be noted that the PtBS42 chain, showing the simplicity in the top panels of Figures 8 and 9, exhibited the thermo-rheological complex behavior in the previously examined PI53/PtBS42 blend[38] because the relaxation time of the PI53 chain therein approached the PtBS42 relaxation time at high T.)

The top panel of Figure 10 shows the T dependence of the shift factor $a_{T,G}$ utilized for the low-M_{PI} blends in Figures 8 and 9. (The shift factor was the same for $G^{bld}_{PtBS}*(\omega)$ and $G^{bld}_{PtBS}(t)$.) The data for these blends agree with each other, which demonstrates that τ_s of the Rouse segment of PtBS is determined by the chemical composition irrespective of M_{PtBS}. The $a_{T,G}$ data for the PI3/PtBS42 reference blend (shown with the diamond) exhibit slightly weaker T dependence because the oligomeric PI3 plasticizes the PtBS chains more strongly than the PI20 chains.

The $a_{T,G}$ data shown in the top panel of Figure 10 were subjected to the WLF analysis to determine the iso-τ_s temperatures $T_{iso\text{-}PtBS}$ for PtBS. Specifically, $T_{iso\text{-}PtBS}$ for the PtBS chains in the blends, corresponding to $T^{bulk}_{iso-PI} = 180^\circ C$ of bulk PtBS, was found to be:

$$T_{iso\text{-}PtBS} = 25^\circ C \text{ in the PI20/PtBS42 and PI20/PtBS70 blends} \qquad (12a)$$

$$T_{iso\text{-}PtBS} = 22^\circ C \text{ in the PI3/PtBS42 blend} \qquad (12b)$$

The difference between these $T_{iso\text{-}PtBS}$ values, 3˚C, reflects an extra plasticization of PtBS due to the oligomeric PI3. Thus, for the PI20/PtBS42 and PI20/PtBS70 blends at a given T, the non-entangled PI3/PtBS42 blend is in the iso-τ_s state at a temperature of T–3. In the bottom panel of Figure 10, the shift factor re-evaluated for these $T_{iso\text{-}PtBS}$, $a_{T,iso\text{-}PtBS}$, is plotted against a temperature difference, $T-T_{iso\text{-}PtBS}$. The $a_{T,iso\text{-}PtBS}$ data are indistinguishable for the PtBS chains having the same w_{PI} but different M_{PtBS} (PtBS42 and PtBS70) and are well described by the WLF equation for bulk PtBS shown with the solid curve (cf. Appendix):

$$\log a_T = -\frac{10.0(T - T_{iso\text{-}PtBS})}{116.5 + T - T_{iso\text{-}PtBS}} \quad (\text{with } T^{bulk}_{iso-PtBS} = T_{r,bulk} = 180^\circ C) \qquad (13)$$

Now, the relaxation mechanism is examined for the PtBS chains in the PI20/PtBS42 and PI20/PtBS70 blends. For this purpose, the G^* data of the non-entangled PI3/PtBS42 reference blend are useful. In the top panel of Figure 8, the data of this reference blend at 17˚C (in the iso-τ_s state corresponding to the PI20/PtBS42 blend at 20˚C) are shown with the dotted curves. The behavior of the PtBS70 chain in the non-entangled iso-τ_s state can be estimated by reducing and

shifting the G^* data of the reference blend by the Rouse factors, that is, by the intensity reduction factor of M_{PtBS42}/M_{PtBS70} (= 0.60) and the shifting factor of $\{M_{PtBS42}/M_{PtBS70}\}^2$ (= 0.36) along the ω axis. The reference G^* data for the PtBS70 chain thus obtained are shown with the dotted curves in the bottom panel of Figure 8. These reference G^* data for the PtBS42 and PtBS70 chains were converted to the relaxation modulus $G(t)$ with the previously reported iteration method.[42] The dotted curves in Figure 9 show the reference $G(t)$ data thus obtained.

Clearly, the PtBS relaxation in the non-entangled, iso-τ_s state is faster, by a factor of $\cong 5$, compared to that in the PI20/PtBS blends. This fact, noted also in the previous study,[26] suggests that the PtBS relaxation is retarded by the moderately entangling PI20 chains. The PI20 chain penetrates into (or *stitches*) neighboring PtBS chains to constrain the motion of these PtBS chains that are not entangled among themselves.[26]

In Figure 8, the solid curves indicate the reference G^* data in the non-entangled, iso-τ_s state that were shifted to lower ω to match the low-ω tails of the $G^{bld}_{PtBS}{}^*(\omega)$ data for the PI20/PtBS42 and PI20/PtBS70 blends. The solid curves in Figure 9 show the reference $G(t)$ data shifted to match the long-t tails of the $G^{bld}_{PtBS}(t)$. These curves agree well with the $G^{bld}_{PtBS}{}^*(\omega)$ and $G^{bld}_{PtBS}(t)$ data in the range of ω and t examined (where Eq. 6 based on the entanglement concept is valid). This agreement suggests that the PtBS42 and PtBS70 chains in those blends exhibit the retarded Rouse-like relaxation attributable to a *pseudo-constraint release* (pseudo-CR) mechanism discussed previously.[26] Namely, the PtBS chains moderately entangled with (or stitched by) the PI20 chains relax on the global motion of the PI20 chain.

In relation to this relaxation mechanism, it should be emphasized that the PI20 chain fully relaxes immediately after its Rouse equilibration within the entanglement length a, as evidenced from the coincidence of ω_x (= ω_ε) and ω_a explained earlier for Figure 1. Because the full relaxation of PI20 completing at $\omega_x = \omega_a$ activates the Rouse-type pseudo-CR process for the PtBS chain, this process occurs smoothly after the Rouse equilibration of the PtBS chain at ω_a without a time lag. This lack of the time lag results in a monotonic change of the ω dependence of the G^* data of the blend, without a hump in the G'' curve explained earlier, from the Rouse equilibration regime to the pseudo-CR regime. (In relation to this point, it should be also noted that the G^* data of the blend at $\omega >> \omega_a$ were contributed from the PI20 chain and not in perfect agreement with the G^* data of the entanglement-free reference system shown with the dotted curves in Figures 8 and 9.)

3.5 Relaxation mechanism of PtBS in blends with $\tau_G \sim \tau_\varepsilon$

$G_{\rm PtBS}^{\rm bld}$* cannot be accurately evaluated for the PI99/PtBS42 blend because the PI99 chain significantly contributes to the terminal viscoelastic relaxation of this blend, in particular at high T, as explained earlier. Thus, the thermo-rheological behavior of the PtBS42 chain cannot be examined for this blend. Nevertheless, at low T (20˚C) where the Rouse equilibration frequency ω_a was experimentally determined (cf. thin arrow in Figure 4), the G^* data of the blend as a whole can be examined to test the relaxation mechanism of the PtBS42 chain, as discussed below.

In the PI99/PtBS42 blend, the PtBS42 chains are not entangled among themselves (cf. Eq. 11) but with the PI99 chains (cf. Eq. 2). As noted in Figure 4, the PI99 chains at 20˚C exhibit the entanglement relaxation significantly slower than the Rouse equilibration; compare ω_ε ($\cong \omega_{\rm x}$ for the cross of the $\Delta\varepsilon'$ and ε'' curves) and ω_a. Consequently, the PtBS42 chains in the blend appear to first relax partly through the Rouse equilibration within the entanglement segment (together with the PI99 chains) and then completely through the pseudo-CR mechanism activated by the global motion of the PI99 chains. Differing from the situation in the low-$M_{\rm PI}$ blends (having $\omega_\varepsilon \cong \omega_a$), the PI99/PtBS42 blend has $\omega_\varepsilon << \omega_a$, and thus the pseudo-CR process therein should have occurred well after the Rouse equilibration.

On the basis of the above molecular picture, the modulus of the PI99/PtBS42 blend in the entire range of ω is expected to be described by a model previously proposed for entangled PI/PtBS blends,[27] $G_{\rm blend}^*(\omega) = G_{\rm PI}^{\rm bld}*(\omega) + G_{\rm PtBS}^{\rm bld}*(\omega)$, where the PI and PtBS moduli, $G_{\rm PI}^{\rm bld}*(\omega)$ and $G_{\rm PtBS}^{\rm bld}*(\omega)$, are given by:[27]

$$G_{\rm PI}^{\rm bld}*(\omega) = \frac{C_{\rm PI}RT}{M_{\rm e,PI}}\sum_{p=1}^{N_{\rm R}} \frac{i\omega\tau_a / r_p^2}{1+i\omega\tau_a / r_p^2} + \phi_{\rm PI} I_{\rm PI} G_{\rm PI}^{\rm bulk}*(\omega\lambda_{\rm PI}Q^{2.33}) \qquad (14a)$$

with

$$r_p = \sin\left\{\frac{p\pi}{2(N_{\rm R}+1)}\right\}\sin^{-1}\left\{\frac{\pi}{2(N_{\rm R}+1)}\right\} \qquad (14b)$$

and

$$G_{\rm PtBS}^{\rm bld}*(\omega) = \frac{C_{\rm PtBS}RT}{M_{\rm e,PtBS}}\sum_{p=1}^{N_{\rm R}} \frac{i\omega\tau_a / r_p^2}{1+i\omega\tau_a / r_p^2} + \frac{C_{\rm PtBS}RT}{M_{\rm PtBS}}\sum_{p=1}^{N_{\rm CR}-1} \frac{i\omega\tau_{\rm CR} / q_p^2}{1+i\omega\tau_{\rm CR} / q_p^2} \qquad (15a)$$

with

$$q_p = \sin\left\{\frac{p\pi}{2N_{\rm CR}}\right\}\sin^{-1}\left\{\frac{\pi}{2N_{\rm CR}}\right\} \qquad (15b)$$

In Eq. 14a, the first summation term, dominating $G_{\rm PI}^{\rm bld}*(\omega)$ at $\omega > \omega_a$, indicates the modulus for the Rouse equilibration process having the mode relaxation time ratio r_p (Eq. 14b) and the slowest

mode relaxation time τ_a (= $1/\omega_a$; determined in Figure 4). The number of the Rouse segments per entanglement segment N_R is evaluated from $M_{e,PI}$ (= 5.7×10^3 in the blend; cf. Eq. 2) and the molecular weight of the Kuhn segment of PI, $M_{K,PI}$ (= 130),[37] as $N_R = M_{e,PI}/M_{K,PI} = 43$. The second $\phi_{PI} I_{PI} G_{PI}^{bulk} *(\omega\lambda_{PI} Q^{2.33})$ term is identical to the modulus $G_{PI,e}^{bld} *(\omega)$ for the entanglement relaxation of PI99 that has been evaluated earlier and shown in Figure 4 with the solid curves.

As for the PtBS modulus, the first summation term in Eq.15a represents the Rouse equilibration process common for PtBS42 and PI99 chains. The second summation term indicates the modulus for the pseudo-CR process that is modeled as the usual Rouse-type CR process[44] for N_{CR} entanglement segments per PtBS42 chain ($N_{CR} = M_{PtBS}/M_{e,PtBS} = 4$). The mode relaxation time ratio for this process, q_p, is described by Eq.15b. On the basis of the Graessley model,[44] the terminal CR time, τ_{CR}, can be related to the terminal viscoelastic relaxation time τ_G^{PI} of the PI99 chain activating the CR process:

$$\tau_{CR} = q_{N_{CR}-1}^2 \Lambda(z) \tau_G^{PI} \quad \text{with} \quad \Lambda(z) = \frac{1}{z}\left(\frac{\pi^2}{12}\right)^z \tag{16}$$

The $q_{N_{CR}-1}$ factor is given by Eq.15b with $p = N_{CR}-1$, τ_G^{PI} is evaluated for the $G_{PI,e}^{bld} *(\omega)$ curve shown in Figure 4, and z is the local jump gate number typically in a range of z = 2-4.[44]

The model explained above is essentially identical to the previous model[27] developed for the high-M PI/PtBS blends in which the PI chains relax much faster than the PtBS chains (to have $\tau_G^{PI} = \tau_\varepsilon^{PI}$) and the PtBS chains are highly entangled with the PI chains as well as among themselves. However, in the PI99/PtBS42 blends examined in this study, the PI99 relaxation is just moderately faster than the PtBS42 relaxation (compare ω_x and ω_G at 20˚C shown in Figure 4) and the PtBS42 chains are not entangled among themselves. According to these differences, the previous model was modified by utilizing $\tau_G^{PI} \cong \tau_\varepsilon^{PI}/2$ in Eq.16 (instead of $\tau_G^{PI} = \tau_\varepsilon^{PI}$ for the case of CR/DTD suppression in the high-M blends) and eliminating the PtBS-PtBS entanglement plateau considered in that model.

The values of model parameters appearing in Eqs. 14-16 are summarized in Table 2. The parameters, except the local jump gate number z, were known and/or evaluated from experimental data, as shown in the footnote of Table 2. The previous study[27] suggested that the data of several high-M PI/PtBS blends were well described by the model with z = 2 (a value in the typical range of z). Thus, z = 2 was also utilized in this study to calculate $G_{blend} *(\omega) = G_{PI}^{bld} *(\omega) + G_{PtBS}^{bld} *(\omega)$ from eqs 14-16. In Figure 11, the calculated and measured $G_{blend} *$ are shown with the solid curves and

symbols, respectively. Although the model does not reproduce the weak and slow relaxation reflected in the $G_{\rm blend}'$ data at low ω, it describes well the dominant part of the $G_{\rm blend}^*(\omega)$ data including the hump of $G_{\rm blend}''$ at ω = 0.3-0.03 s^{-1} explained earlier for Figure 4. This result lends support to the molecular picture underlying the model; that is, the cooperative Rouse equilibration of the PI and PtBS chains followed by the considerably slower entanglement relaxation of PI and the pseudo-CR relaxation of PtBS activated by this PI relaxation.

Finally, one may attempt to apply the above model also to the low-$M_{\rm PI}$ PI20/PtBS blends at 20˚C. However, it should be noted that the local CR process incorporated in the model can occur only after the entanglement segment is equilibrated.[44] In the high-$M_{\rm PI}$ PI99/PtBS42 blend, the Rouse-equilibration time, τ_a (= 0.4 s; Table 1) is much shorter than $\Lambda(z)\tau_G^{\rm PI}$ (= 3.4 s), so that the CR-onset time τ^* can be evaluated as $\tau^* = \Lambda(z)\tau_G^{\rm PI}$ (cf. Eq.16).[44] In contrast, the low-$M_{\rm PI}$ blends have $\tau_a \cong \tau_\varepsilon^{\rm PI} > \Lambda(z)\tau_G^{\rm PI}$ (cf. Figure 1) and their τ^* cannot be evaluated in the same way. Thus, the above model needs to be modified for the low-$M_{\rm PI}$ blends. The pseudo-CR process for the PtBS chain in the low-$M_{\rm PI}$ blends occurs smoothly after the Rouse equilibration, as explained earlier. Thus, in the approximate but simplest modification, we may express the PtBS modulus, $G_{\rm PtBS}^{\rm bld}*(\omega)$, in the Rouse form for the relaxation of a whole sequence of N Rouse segments in the PtBS chain ($N = M_{\rm PtBS}/M_{\rm K} >> 1$):

$$G_{\rm PtBS}^{\rm bld}*(\omega) = \frac{C_{\rm PtBS}RT}{M_{\rm PtBS}}\sum_{p=1}^{N-1}\frac{i\omega\tau_{\rm CR}/q_p'^2}{1+i\omega\tau_{\rm CR}/q_p'^2} \tag{17a}$$

with

$$q_p' = \sin\left\{\frac{p\pi}{2N}\right\}\sin^{-1}\left\{\frac{\pi}{2N}\right\} \tag{17b}$$

The terminal CR time $\tau_{\rm CR}$ in Eq.17a is treated as an adjustable parameter (instead of z appearing in Eq.16). The PI modulus, $G_{\rm PI}^{\rm bld}*(\omega)$, is not affected by this modification and is given by Eq.14 with the second term being replaced by $G_{\rm PI,e}^{\rm bld}*(\omega)$ of PI20 (shown in the top panel of Figure 2 with the solid curves).

The parameters included in the modified model explained above are τ_a, $N_{\rm R}$, N (= $N_{\rm R}N_{\rm CR}$), and $\tau_{\rm CR}$. The first three parameters were determined experimentally in a way explained in the footnote of Table 2; τ_a = 0.4 s, $N_{\rm R}$ = 43, and N = 172. (These values are the same as those shown in Table 2 for the high-$M_{\rm PI}$ PI99/PtBS42 blend.) $\tau_{\rm CR}$ was used as the adjustable parameter to calculate $G_{\rm blend}^*(\omega) = G_{\rm PI}^{\rm bld}*(\omega) + G_{\rm PtBS}^{\rm bld}*(\omega)$ for the PI20/PtBS42 blend. As shown in Figure 12, the

calculated G_{blend}* (for τ_{CR} = 20 s; solid curves) can mimic the data (symbols) considerably well, although non-trivial deviation (possibly due to the oversimplification of the model) is still noted. This result further confirms the validity of the molecular picture, the cooperative Rouse equilibration of the PI and PtBS chains followed by the entanglement relaxation of PI (that occurs immediately after the equilibration for the case of the low-M_{PI} PI20/PtBS42 blend) and further by the pseudo-CR relaxation of PtBS activated by this PI relaxation. Thus, the relaxation behavior of the low-M_{PI} and high-M_{PI} blends can be described and understood on a common basis.

4 CONCLUDING REMARKS

The viscoelastic and dielectric behavior was examined for the moderately entangled PI/PtBS blends (w_{PI} = 55.7 wt%) in the miscible state to investigate the thermo-rheological behavior and the relaxation mechanisms of the component chains therein. The dielectric data of the blends exclusively detected the global motion of the PI chains having the type-A dipole. Comparison of the dielectric and viscoelastic data indicated that the global motion of the PI chain was much faster than that of the PtBS chain in the low-M_{PI} PI20/PtBS42 and PI20/PtBS70 blends, whereas the motion of these chains was equally slow in the high-M_{PI} PI99/PtBS42 blend.

The dielectrically detected PI dynamics exhibited the thermo-rheological complexity, in particular in the low-M_{PI} blends. This complexity was attributable to the dynamic frictional heterogeneity quenched by the slow PtBS chains in the time scale of the PI relaxation. The PI chains appeared to exhibit the entanglement relaxation affected by this frictional heterogeneity as well as the topological constraint from the slow PtBS chains.

For the low-M_{PI} blends, the viscoelastic data in the terminal relaxation regime were dominated by the slow PtBS chains. The PtBS modulus, $G^{bld}_{PtBS}*(\omega)$ and/or $G^{bld}_{PtBS}(t)$, in those blends at low ω and/or long t, being indistinguishable from the blend modulus and evaluated with negligible uncertainty, satisfied the time-temperature superposition. This thermo-rheological simplicity was attributed to the fast PI chains that smeared the frictional heterogeneity during the slow terminal relaxation of PtBS. Nevertheless, the PtBS chains showed no ordinary entanglement relaxation associated with the G' plateau but exhibited Rouse-like relaxation that was slower, by a factor of $\cong$5, than the relaxation in a non-entangled, iso-τ_s reference state. This retarded Rouse-like relaxation of PtBS was attributable to the pseudo-constraint release mechanism activated by the

global motion of the PI chains entangling with the PtBS chains. A simple model considering this mechanism described the G^* data of the low-M_{PI} and high-M_{PI} blends considerably well.

Acknowledgment: This work was supported by the Collaborative Research Program of Institute for Chemical Research, Kyoto University (grant # 2010-32), a Grant-in-Aid for Scientific Research on Priority Area "Soft Matter Physics" from MEXT (grant #18068009), and a Grant-in-Aid for Young Scientists (B) from MEXT (grant #22750204). QC is thankful for support from JSPS.

Appendix. Dynamic behavior of bulk PI and PtBS

The viscoelastic and dielectric behavior was examined for the PI and PtBS components in respective bulk states. Figure 13 shows the master curves of $G', G'', \Delta\varepsilon'$, and ε'' measured for those bulk PI, and Figure 14 shows the curves of G' and G'' measured for those bulk PtBS. The PI chain has the type-A dipole, and thus its global motion activates the viscoelastic and dielectric terminal relaxation in the same range of ω. Consequently, the shift factor a_T was the same for the viscoelastic and dielectric data of PI and was described by the previously reported WLF equation:[26]

$$\log a_T = -\frac{4.425(T - T_{r,bulk})}{140.0 + T - T_{r,bulk}} \quad \text{with } T_{r,bulk} = 30^\circ\text{C for bulk PI} \qquad \text{(A1)}$$

In contrast, the PtBS chain has no type-A dipole, and its global motion is dielectrically inert. The shift factor a_T for the viscoelastic data of PtBS was described by the previously reported WLF equation:[26]

$$\log a_T = -\frac{10.0(T - T_{r,bulk})}{116.5 + T - T_{r,bulk}} \quad \text{with } T_{r,bulk} = 180^\circ\text{C for bulk PtBS} \qquad \text{(A2)}$$

Table 1. Characteristics of Samples

Code	$10^{-3}M_w$	M_w/M_n
cis-polyisoprene (PI)		
PI3	3.0	1.07
PI20	19.9	1.10
PI53	53.4	1.03
PI99	98.5	1.04
poly(*p*-*tert*-butyl styrene) (PtBS)		
PtBS42	41.8	1.04
PtBS70	69.5	1.03

Table 2. Parameters used in the model for PI99/PtBS42 (w_{PI} = 55.7 wt%) at 20˚C; cf. Eqs. 14-16.

τ_a/s [a]	0.4
τ_G^{PI}/s [b]	10.0
$10^{-3} M_{e,PI}$ [c]	5.7
$10^{-3} M_{e,PtBS}$ [c]	10.5
N_R [d]	43
N_{CR} [e]	4
τ_{CR}/s [f]	23.0
z [g]	2

a: evaluated from G^* data (cf. Eq. 8)

b: estimated from the modulus data for the entanglement relaxation of PI, $G_{PI,e}^{bld}(\omega) = \phi_{PI} I_{PI} G_{PI}^{bulk} * (\omega \lambda_{PI} Q^{2.33})$, shown in Figure 4.

c: given by Eq. 2

d: $N_R = M_e^{PI} / M_{K,PI}$

e: $N_{CR} = M_{PtBS} / M_{e,PtBS}$

f: evaluated from τ_G^{PI} and z (cf. Eq. 16)

g: z value utilized in Ref. 27

References

1. Miller, J. B., McGrath, K. J., Roland, C. M., Trask, C. A., Garroway, A. N. Nuclear Magnetic Resonance Study of Polyisoprene Poly(vinylethylene) Miscible Blends. *Macromolecules* **23**, 4543-4547 (1990).
2. Chung, G. C., Kornfield, J. A., Smith, S. D. Component Dynamics in Miscible Polymer Blends: A Two-Dimensional Deuteron NMR Investigation. *Macromolecules* **27,** 964-973 (1994).
3. Alegria, A., Colmenero, J., Ngai, K. L., Roland, C. M. Observation of the Component Dynamics in a Miscible Polymer Blend by Dielectric and Mechanical Spectroscopies. *Macromolecules* **27**, 4486-4492 (1994).
4. Kumar, S. K., Colby, R. H., Anastasiadis, S. H., Fytas, G. Concentration Fluctuation induced Dynamic Heterogeneities in Polymer Blends. *J. Chem. Phys.* **105,** 3777-3788 (1996).
5. Wetton, R. E., MacKnight, W. J., Fried, J. R., Karasz, F. E. Compatibility of Poly(2,6-dimethyl-1,4-phenylene oxide) (PPO)/Poly(styrene-co-4-chlorostyrene) Blends. 2. Dielectric Study of the Critical Composition Region. *Macromolecules* **11**, 158-165 (1978).
6. Liang, K. M., Banhegyi, G., Karasz, F. E., Macknight, W. J. Thermal, Dielectric, and Mechanical Relaxation in Poly(benzimidazole)/Poly(etherimide) Blends. *J. Polym. Sci. Part B: Polym. Phys.* **29**, 649-657 (1991).
7. Miura, N., MacKnight, W. J., Matsuoka, S., Karasz, F. E. Comparison of Polymer Blends and Copolymers by Broadband Dielectric Analysis. *Polymer* **42**, 6129-6140 (2001).
8. He, Y. Y., Lutz, T. R., Ediger, M. D. NMR Investigation of Segmental Dynamics in Disordered Styrene-Isoprene Tetrablock Copolymers. *Macromolecules* **36**, 8040-8048 (2003).
9. He, Y. Y., Lutz, T. R., Ediger, M. D. Comparison of the Composition and Temperature Dependences of Segmental and Terminal Dynamics in Polybutadiene/Poly(vinyl ethylene) Blends. *Macromolecules* **37**, 9889-9898 (2004).
10. Zhao, J. S., Ediger, M. D., Sun, Y., Yu, L. Two DSC Glass Transitions in Miscible Blends of Polyisoprene/Poly(4-tert-butylstyrene). *Macromolecules* **42**, 6777-6783 (2009).
11. Angell, C. A. Perspective on the Glass Transition. *J. Phys. Chem. Solids* **49**, 863-971 (1988).
12. Hodge, I. M. Strong and Fragile Liquids - A Brief Critique. *J. Non-Cryst. Solids* **202**, 164-172 (1996).
13. Roland, C. M., Ngai, K. N. Commentary on 'Strong and Fragile Liquids - A Brief Critique'. *J. Non-Cryst. Solids* **212**, 74-76 (1997).

14. Hirose, Y., Urakawa, O., Adachi, K. Dielectric Study on the Heterogeneous Dynamics of Miscible Polyisoprene/Poly(vinyl ethylene) Blends: Estimation of the Relevant Length Scales for the Segmental Relaxation Dynamics. *Macromolecules* **36**, 3699-3708 (2003).
15. Urakawa, O. Studies on Dynamic Heterogeneity in Miscible Polymer Blends and Dynamics of Flexible Polymers. *Nihon Reoroji Gakkaishi* (*J. Soc. Rheol. Japan*) **32**, 265-270 (2004).
16. Lodge, T. P., McLeish, T. C. B. Self-concentrations and Effective Glass Transition Temperatures in Polymer Blends. *Macromolecules* **33**, 5278-5284 (2000).
17. Zetsche, A., Fischer, E. W. Dielectric Studies of the a-relaxation in Miscible Polymer Blends and its Relation to Concentration Fluctuations. *Acta Polym.* **45**, 168-175 (1994).
18. Pathak, J. A., Colby, R. H., Floudas, G., Jerome, R. Dynamics in Miscible Blends of Polystyrene and Poly(vinyl methyl ether). *Macromolecules* **32**, 2553-2561 (1999).
19. Pathak, J. A., Colby, R. H., Kamath, S. Y., Kumar, S. K., Stadler, R. Rheology of Miscible Blends: SAN and PMMA. *Macromolecules* **31**, 8988-8997 (1998).
20. Pathak, J. A., Kumar, S. K., Colby, R. H. Miscible Polymer Blend Dynamics: Double Reptation Predictions of Linear Viscoelasticity in Model Blends of Polyisoprene and Poly(vinyl ethylene). *Macromolecules* **37**, 6994-7000 (2004).
21. Haley, J. C., Lodge, T. P., He, Y. Y., Ediger, M. D., von Meerwall, E. D., Mijovic, J. Composition and Temperature Dependence of Terminal and Segmental Dynamics in Polyisoprene/Poly(vinylethylene) Blends. *Macromolecules* **36**, 6142-6151 (2003).
22. Haley, J. C., Lodge, T. P. A Framework for Predicting the Viscosity of Miscible Polymer Blends. *J. Rheol.* **48**, 463-486 (2004).
23. Haley, J. C., Lodge, T. P. Viscosity Predictions for Model Miscible Polymer Blends: Including Self-concentration, Double Reptation, and Tube Dilation. *J. Rheol.* **49**, 1227-1302 (2005).
24. Watanabe, H., Matsumiya, Y., Takada, J., Sasaki, H., Matsushima, Y., Kuriyama, A., Inoue, T., Ahn, K. H., Yu, W., Krishnamoorti, R. Viscoelastic and Dielectric Behavior of a Polyisoprene/Poly(4-*tert*-butyl styrene) Miscible Blend. *Macromolecules* **40**, 5389-5399 (2007).
25. Takada, J., Sasaki, H., Matsushima, Y., Kuriyama, A., Matsumiya, Y., Watanabe, H., Ahn, K. H., Yu, W. Component Chain Dynamics in a Miscible Blend of Low-*M* Poly(*p*-*t*-butyl styrene) and Polyisoprene. *Nihon Reoroji Gakkaishi (J. Soc. Rheol. Japan)* **36**, 35-42 (2008).
26. Chen, Q., Matsushima, Y., Masubuchi, Y., Watanabe, H., Inoue, T. Component Dynamics in Polyisoprene/Poly(4-*tert*-butyl styrene) Miscible Blends. *Macromolecules* **41**, 8694-8711 (2008).

27. Watanabe, H., Chen, Q., Kawasaki, Y., Matsumiya, Y., Inoue, T., Urakawa, O. Entanglement Dynamics in Miscible Polyisoprene/Poly(*p*-*tert*-butyl styrene) Blends. *Macromolecules*, *in press* (2011).
28. Watanabe, H. Viscoelasticity and Dynamics of Entangled Polymers. *Prog. Polym. Sci.* **24**, 1253-1403 (1999).
29. Watanabe, H. Dielectric Relaxation of Type-A Polymers in Melts and Solutions. *Macromol. Rapid Commun.* **22**, 127-175 (2001).
30. Yurekli, K., Krishnamoorti, R. Thermodynamic Interactions in Blends of Poly(4-*tert*-butyl styrene) and Polyisoprene by Small-Angle Neutron Scattering. *J. Polym. Sci. Part B: Polym. Phys.* **42**, 3204-3217 (2004).
31. Inoue, T., Okamoto. H., Osaki, K. Birefringence of Amorphous Polymers. 1. Dynamic Measurement on Polystyrene. *Macromolecules* **24**, 5670-5675 (1991).
32. Okamoto, H., Inoue, T., Osaki, K. Viscoelasticity and Birefringence of Polyisoprene. *J. Polym. Sci. Part B: Polym. Phys.* **33**, 417-424 (1995).
33. Inoue, T., Matsui, H., Osaki K. Molecular Origin of Viscoelasticity and Chain Orientation of Glassy Polymers. *Rheol. Acta* **36**, 239-244 (1997).
34. Watanabe, H. Slow Dynamics in Homopolymer Liquids. *Polymer J.* **41**, 929-950 (2009).
35. Fetters, L. J., Lohse, D. J., Richter, D., Witten, T. A., Zirkel, A. Connection between Polymer Molecular Weight, Density, Chain Dimensions, and Melt Viscoelastic Properties. *Macromolecules* **27**, 4639-4647 (1994).
36. Fetters, L. J., Lohse, D. J., Graessley, W. W. Chain Dimensions and Entanglement Spacings in Dense Macromolecular Systems. *J. Polym. Sci. Part B: Polym. Phys.* **37**, 1023-1033 (1999).
37. Fetters, L. J., Lohse, D. J., Colby, R.H. in *Physical Properties of Polymers Handbook* (ed. Mark, J. E.) Ch. 25, 445-452 (Springer, 2007).
38. Chen, Q., Matsumiya, Y., Masubuchi, Y., Watanabe, H., Inoue, T. Dynamics of Polyisoprene-Poly(p-*tert*-butyl styrene) Diblock Copolymer in Disordered State. *Macromolecules*, *in press* (2011).
39. Watanabe, H., Ishida, S., Matsumiya, Y., Inoue, T. Viscoelastic and Dielectric Behavior of Entangled Blends of Linear Polyisoprenes Having Widely Separated Molecular Weights: Test of Tube Dilation Picture. *Macromolecules* **37**, 1937-1951 (2004).
40. Watanabe, H., Ishida, S., Matsumiya, Y., Inoue, T. Test of Full and Partial Tube Dilation Pictures in Entangled Blends of Linear Polyisoprenes. *Macromolecules* **37**, 6619-6631 (2004).

41. Watanabe, H., Sawada, T., Matsumiya Y. Constraint Release in Star/Star Blends and Partial Tube Dilation in Monodisperse Star Systems. *Macromolecules* **39**, 2553-2561 (2006).
42. Watanabe, H., Matsumiya Y., Inoue, T. Dielectric and Viscoelastic Relaxation of Highly Entangled Star Polyisoprene: Quantitative Test of Tube Dilation Model. *Macromolecules* **35**, 2339-2357 (2002).
43. Osaki, K., Inoue, T., Uematsu, T., Yamashita, Y. Evaluation Methods of the Longest Rouse Relaxation Time of an Entangled Polymer in a Semidilute Solution. *J. Polym. Sci. Part B: Polymer Phys.* **39**, 1704-1712 (2001).
44. Graessley, W. W. Entangled Linear, Branched and Network Polymer Systems, Molecular Theories, *Adv. Polym. Sci.* **47**, 67-117 (1982).

Figure Captions

Fig.1

Viscoelastic and dielectric behavior of the PI20/PtBS42 and PI20/PtBS70 blends (w_{PI} = 55.7 wt%) at 20 and 90˚C. The horizontal dashed lines indicate the entanglement plateau modulus G_N expected for the blends. The thick arrows in both top and bottom panels indicate the viscoelastic terminal relaxation frequency of the blends, ω_G, and the thin arrow in the top panel, the frequency ω_a for the Rouse equilibration within the entanglement length a. For further details, see the text.

Fig.2

Comparison of the G_{blend}* data of the PI20/PtBS42 blend (squares) and the modulus $G_{PI,e}^{bld}$ * for the entanglement relaxation of PI20 therein (thick solid curves), the latter being evaluated from the G_{PI}^{bulk} * data of bulk PI20 with the aid of the dielectric data (triangles). The horizontal dashed lines indicate the entanglement plateau modulus G_N expected for the blends. The small filled circles indicate $G_{PtBS}^{bld}*(\omega) = G_{blend}*(\omega) - G_{PI,e}^{bld}*(\omega)$ evaluated in the range of ω where the PI and PtBS chains have been Rouse-equilibrated within the entanglement length. For further details, see the text.

Fig.3

Comparison of the $G_{blend}(t)$ data of the PI20/PtBS42 blend (squares) and the modulus $G_{PI,e}^{bld}(t)$ for the entanglement relaxation of PI20 therein (thick solid curves). Triangles show the dielectric relaxation function $\varepsilon(t)$ multiplied by a factor of 10^4. The horizontal dashed lines indicate the entanglement plateau modulus G_N expected for the blends. The small filled circles indicate $G_{PtBS}^{bld}(t) = G_{blend}(t) - G_{PI,e}^{bld}(t)$ evaluated in the range of t where the PI and PtBS chains have been Rouse-equilibrated within the entanglement length. For further details, see the text.

Fig.4

Viscoelastic and dielectric behavior of the PI99/PtBS42 blend (w_{PI} = 55.7 wt%) at 20, 50, and 90˚C. The horizontal dashed line indicates the entanglement plateau modulus G_N expected for the blend at 20˚C. The thick arrows indicate the viscoelastic terminal relaxation frequency ω_G of the blend at respective T, and the thin arrow, the Rouse equilibration frequency ω_a at 20˚C. Solid curves

indicate the modulus $G^{bld}_{PI,e}$* of PI99 evaluated from the G^{bulk}_{PI}* data of bulk PI99 with the aid of the dielectric data of the blend. For further details, see the text.

Fig.5

Test of thermo-rheological behavior of PI in PI/PtBS blends as indicated. The reference temperature is chosen to be T_r = 90˚C. The dielectric data of the blends (*i.e.*, of the PI chains therein) are shifted along the ω axis to achieve the best superposition at $\omega > \omega_{peak}$. The thick solid curves indicate the dielectric data of bulk PI at 90˚C multiplied by the PI volume fraction in the blend, ϕ_{PI} = 0.59, and shifted along the ω axis to match the ε"-peak frequency ω_{peak} with the blend data. For further details, see the text.

Fig.6

Top panel: Shift factor $a_{T,\varepsilon}$ for the dielectric data of PI in the blends as indicated.

Bottom panel: Shift factor $a_{T,iso\text{-}PI}$ for the dielectric data of PI defined with respect to the iso-τ_s temperature, $T_{iso\text{-}PI}$ = 60˚C. The solid curve indicates the WLF equation for bulk PI with T^{bulk}_{iso-PI} = 30˚C. For further details, see the text.

Fig.7

Viscoelastic behavior of PI3/PtBS42 blend (w_{PI} = 55.7 wt%) at T_r = 20˚C.

Fig.8

Test of time-temperature superposability for the G^{bld}_{PtBS}* data of the PtBS42 and PtBS70 chains in the blends as indicated. The dotted curves show the modulus of these PtBS chains in the entanglement-free, iso-τ_s reference state. For further details, see the text.

Fig.9

Test of time-temperature superposability for the $G^{bld}_{PtBS}(t)$ data of the PtBS42 and PtBS70 chains in the blends as indicated. The dotted curves show the $G(t)$ of these PtBS chains in the entanglement-free, iso-τ_s reference state. For further details, see the text.

Fig.10

Top panel: Shift factor $a_{T,\varepsilon}$ for the viscoelastic data of PtBS in the blends as indicated.

Bottom panel: Shift factor $a_{\mathrm{T,iso\text{-}PtBS}}$ for the viscoelastic data of PtBS defined with respect to the iso-τ_s temperatures as indicated. The solid curve shows the WLF equation for bulk PtBS with $T_{\mathrm{iso-PtBS}}^{\mathrm{bulk}}$ = 180˚C. For further details, see the text.

Fig.11

Comparison of the G^* data of the PI99/PtBS42 blend at 20˚C (symbols) with the model prediction (curves; Eqs. 14-16).

Fig.12

Comparison of the G^* data of the PI20/PtBS42 blend at 20˚C (symbols) with the model prediction (curves; Eqs. 14 and 17).

Fig.13

Viscoelastic and dielectric data of bulk PI utilized as the components in the PI/PtBS blends.

Fig.14

Viscoelastic data of bulk PtBS utilized as the components in the PI/PtBS blends.

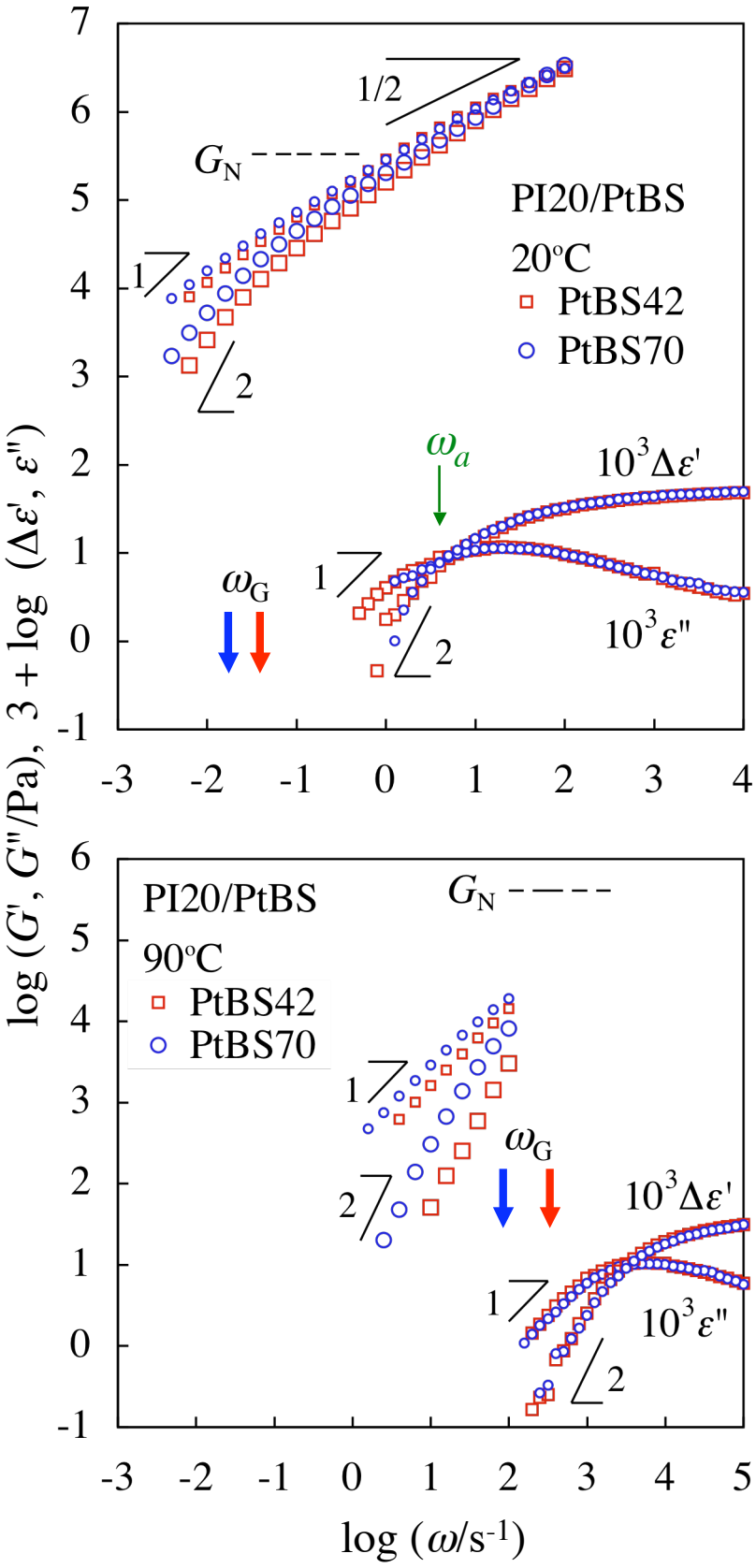
log (G', G"/Pa), 3 + log (Δε', ε")
log (ω/s-1)
PI20/PtBS
20°C
PtBS42
PtBS70
GN
1/2
1
2
ωa
ωG
10³Δε'
10³ε"
PI20/PtBS
90°C
PtBS42
PtBS70
GN

Fig.1

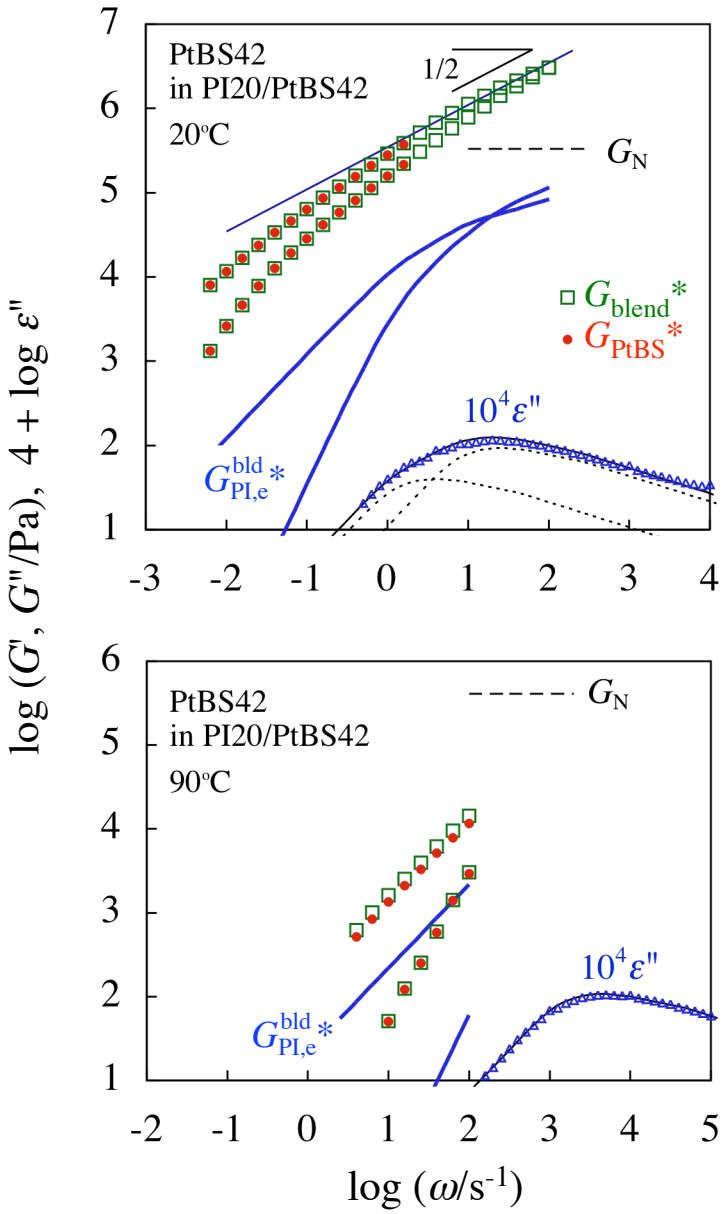
PtBS42
in PI20/PtBS42
20°C
1/2
G_N
G_{blend}*
G_{PtBS}*
$10^4\varepsilon''$
$G_{PI,e}^{bld}$*
PtBS42
in PI20/PtBS42
90°C
G_N
$10^4\varepsilon''$
$G_{PI,e}^{bld}$*
log (G', G''/Pa), 4 + log ε''
log (ω/s^{-1})

Fig.2

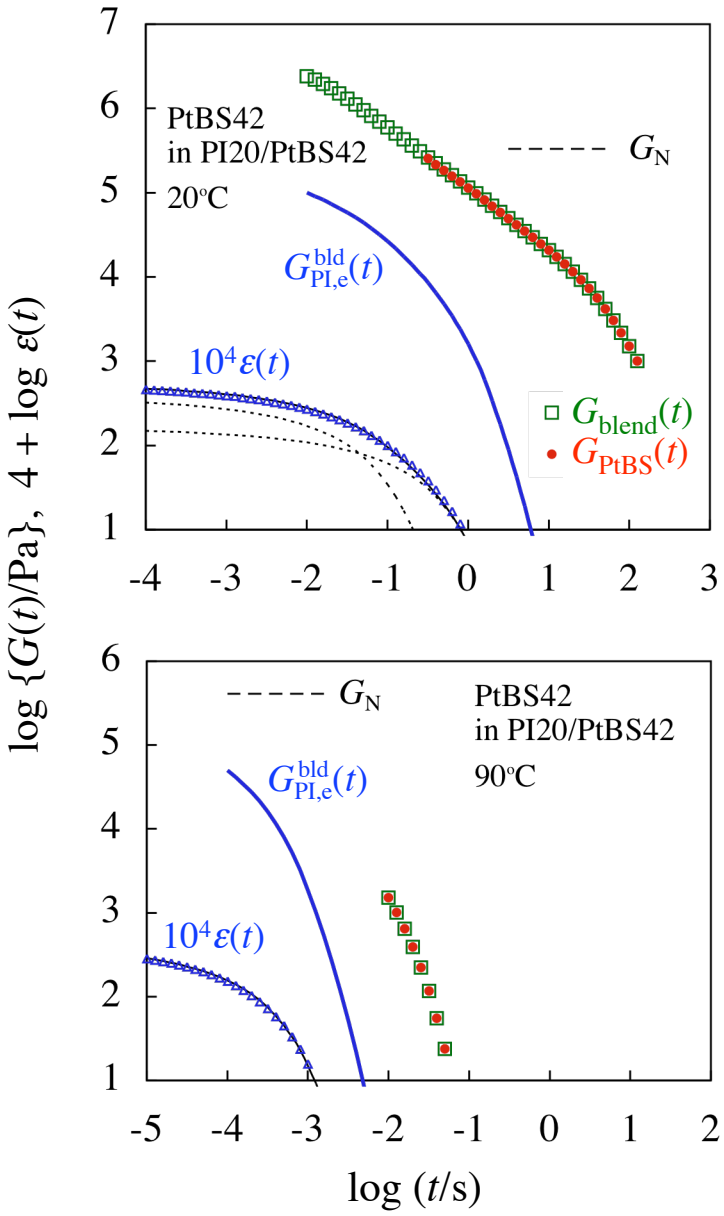
PtBS42
in PI20/PtBS42
20°C
G_N
$G_{PI,e}^{bld}(t)$
$10^4\varepsilon(t)$
$G_{blend}(t)$
$G_{PtBS}(t)$
PtBS42
in PI20/PtBS42
90°C
log {$G(t)$/Pa}, 4 + log $\varepsilon(t)$
log (t/s)

Fig.3

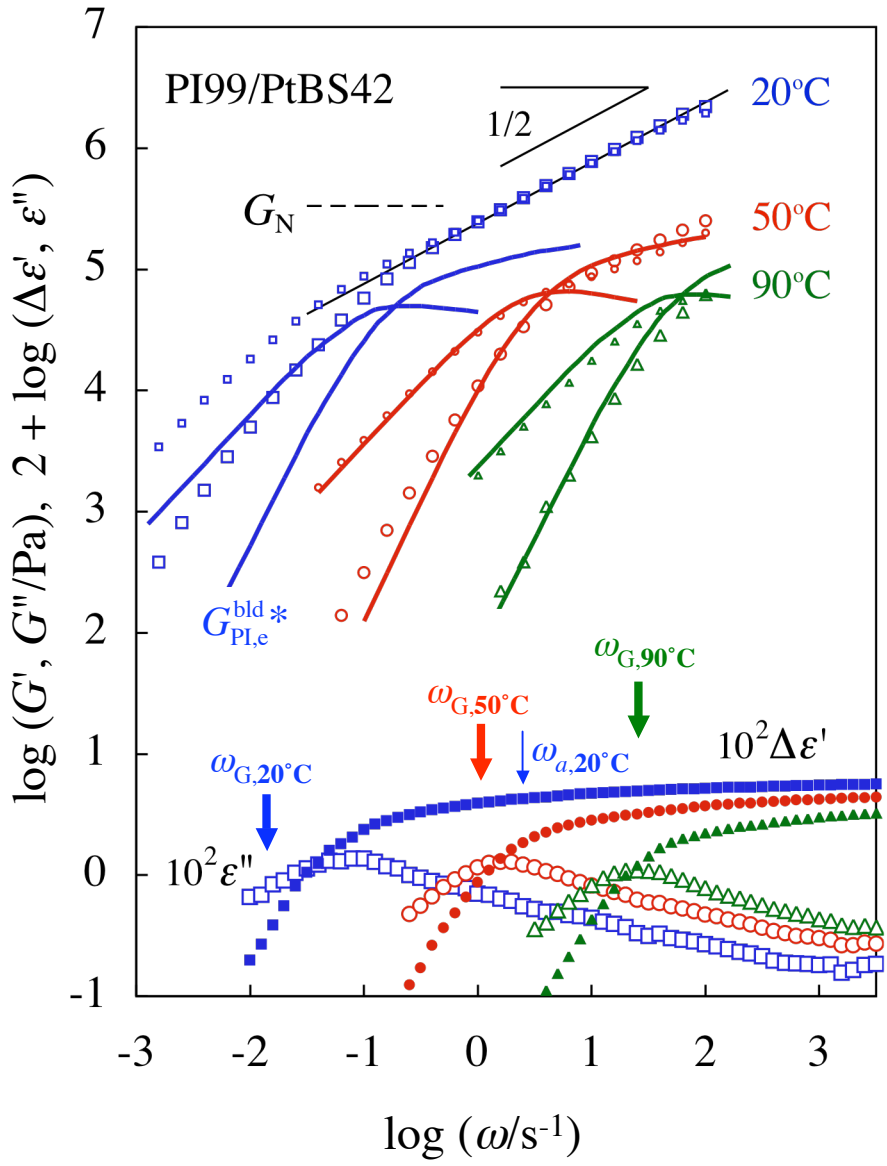
PI99/PtBS42
1/2
20°C
50°C
90°C
G_N
$G^{bld}_{PI,e}$ *
$\omega_{G,90°C}$
$\omega_{G,50°C}$
$\omega_{a,20°C}$
$\omega_{G,20°C}$
$10^2\Delta\varepsilon'$
$10^2\varepsilon''$
log (G', G''/Pa), 2 + log (Δε', ε'')
log (ω/s^{-1})
7
6
5
4
3
2
1
0
-1
-3
-2
-1
0
1
2
3

Fig.4

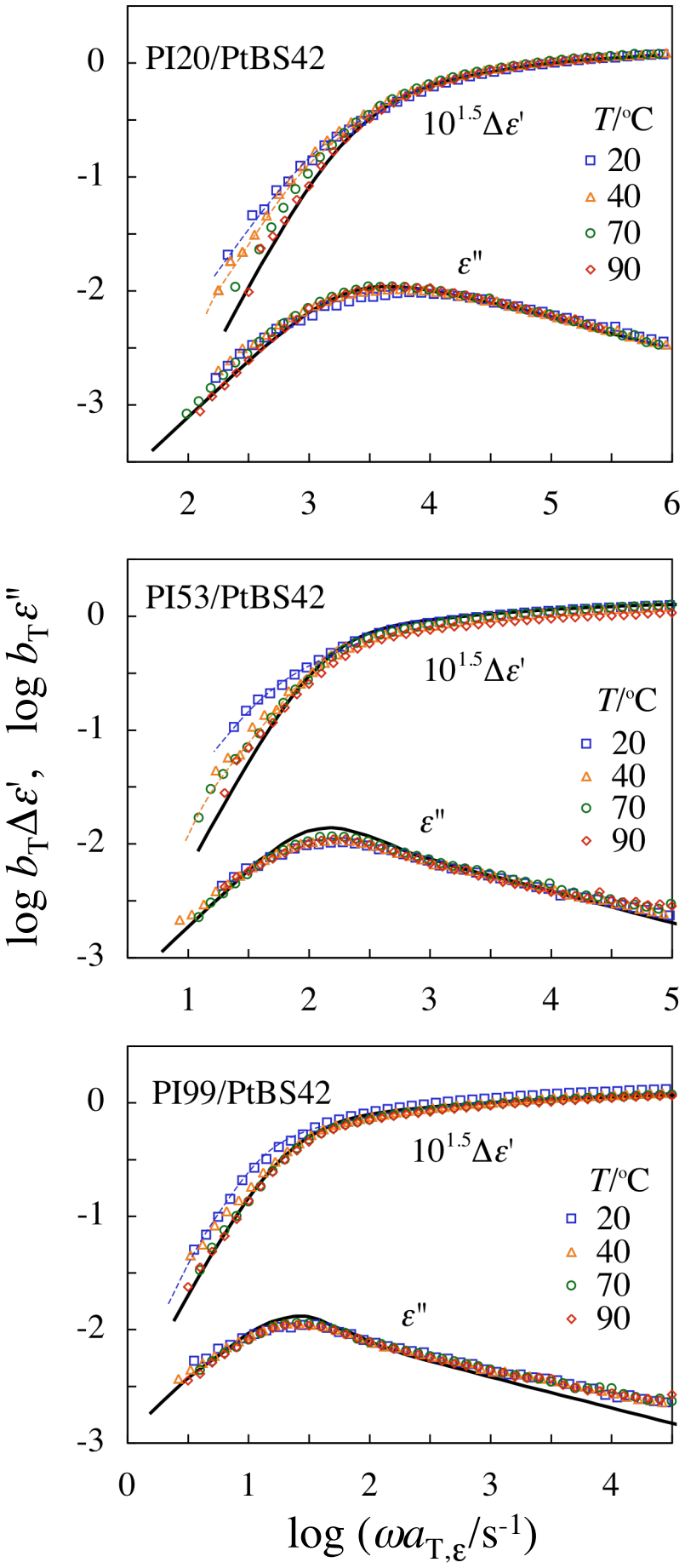
PI20/PtBS42
$10^{1.5}\Delta\varepsilon'$
T/°C
20
40
70
90
ε"
PI53/PtBS42
$10^{1.5}\Delta\varepsilon'$
T/°C
20
40
70
90
ε"
PI99/PtBS42
$10^{1.5}\Delta\varepsilon'$
T/°C
20
40
70
90
ε"
log $b_T\Delta\varepsilon'$, log $b_T\varepsilon$"
log ($\omega a_{T,\varepsilon}$/s^{-1})

Fig.5

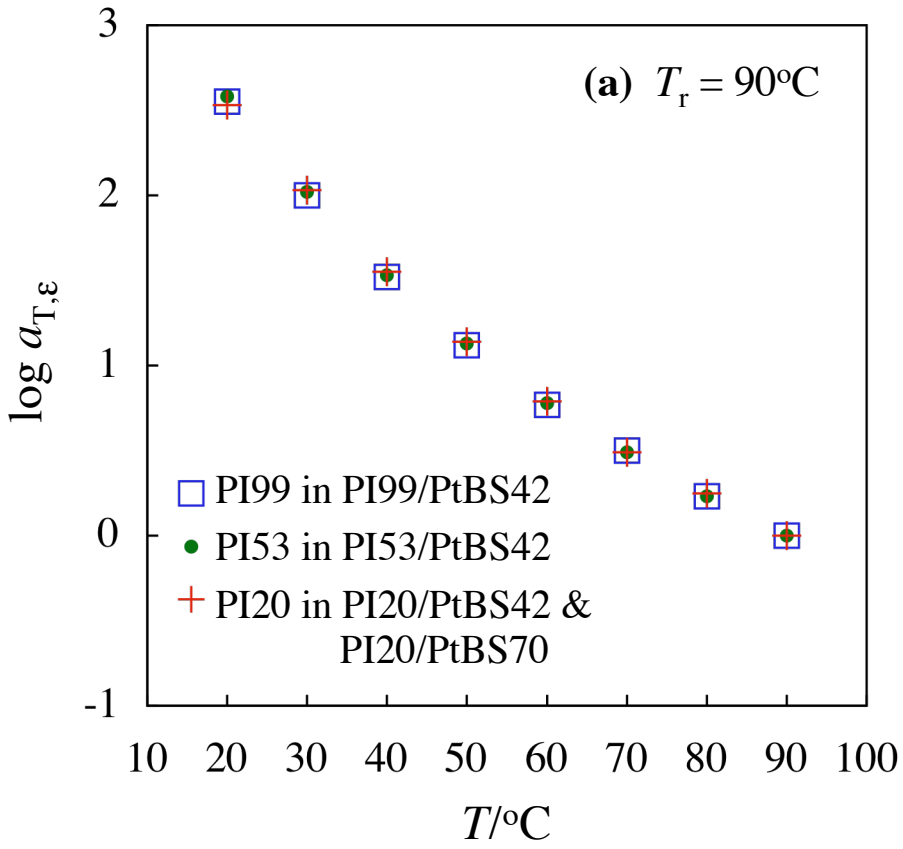
(a) T_r = 90°C
log $a_{T,\varepsilon}$
PI99 in PI99/PtBS42
PI53 in PI53/PtBS42
PI20 in PI20/PtBS42 &
PI20/PtBS70
T/°C

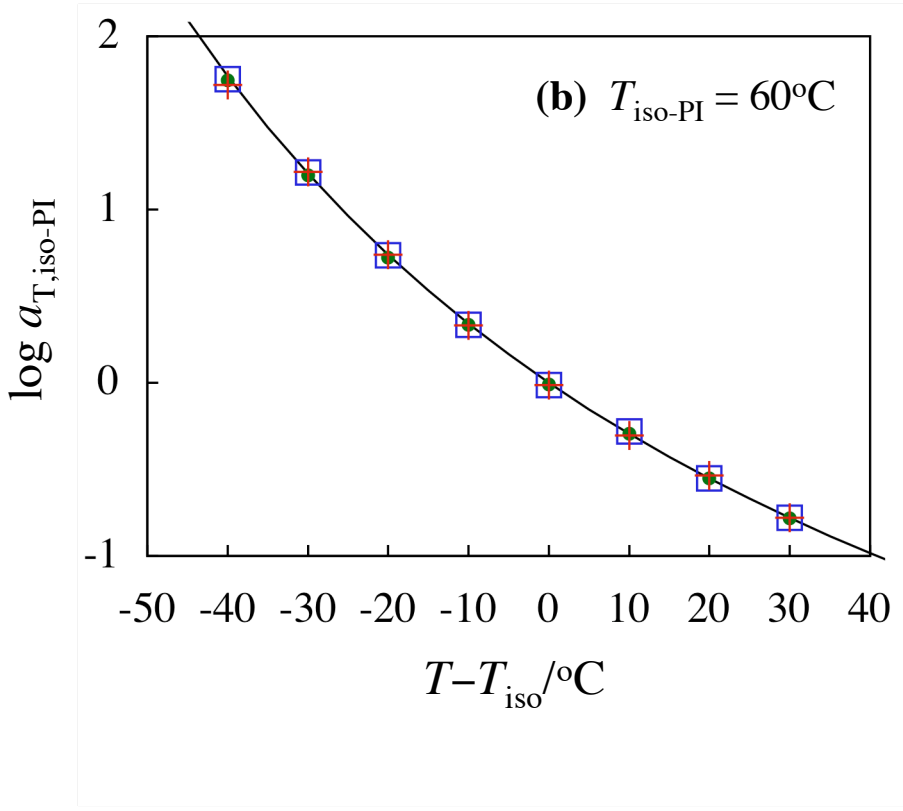
(b) $T_{iso\text{-}PI}$ = 60°C
log $a_{T,iso\text{-}PI}$
$T-T_{iso}$/°C

Fig.6

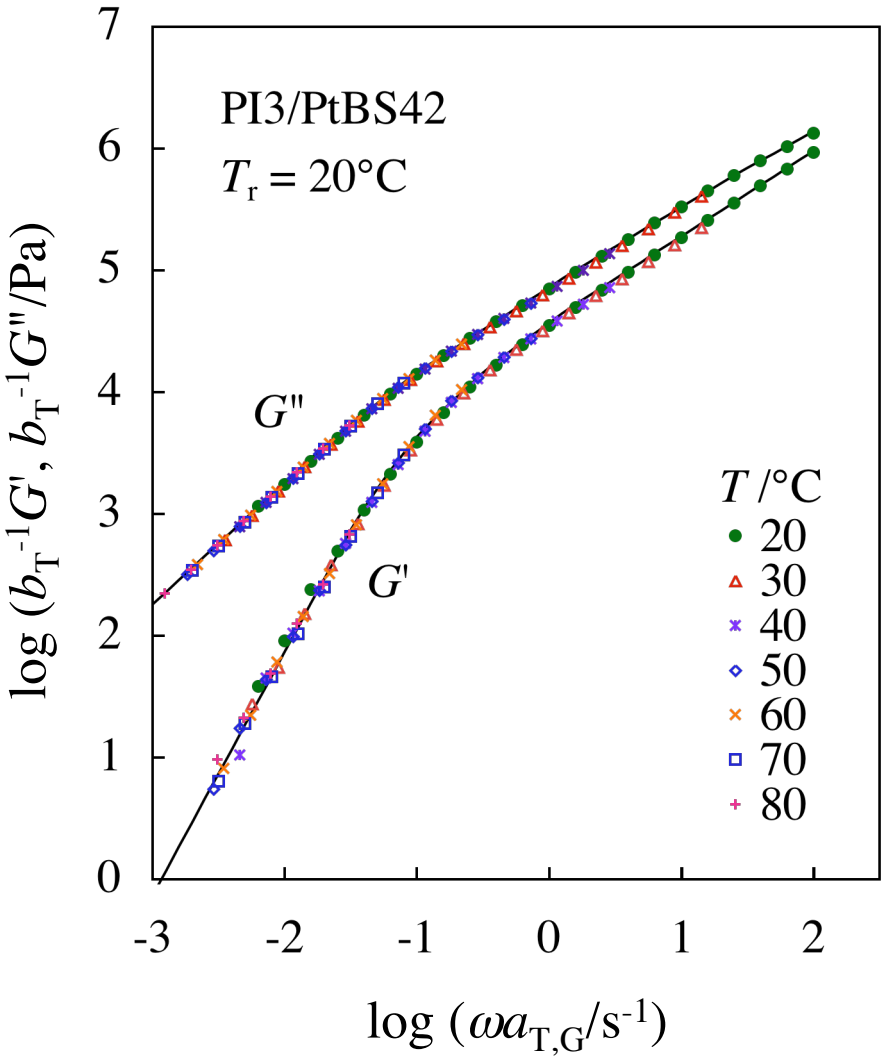
PI3/PtBS42
T_r = 20°C
G''
G'
T /°C
20
30
40
50
60
70
80
log ($b_T^{-1}G'$, $b_T^{-1}G''$/Pa)
log ($\omega a_{T,G}$/s^{-1})
0
1
2
3
4
5
6
7
-3
-2
-1
0
1
2

Fig.7

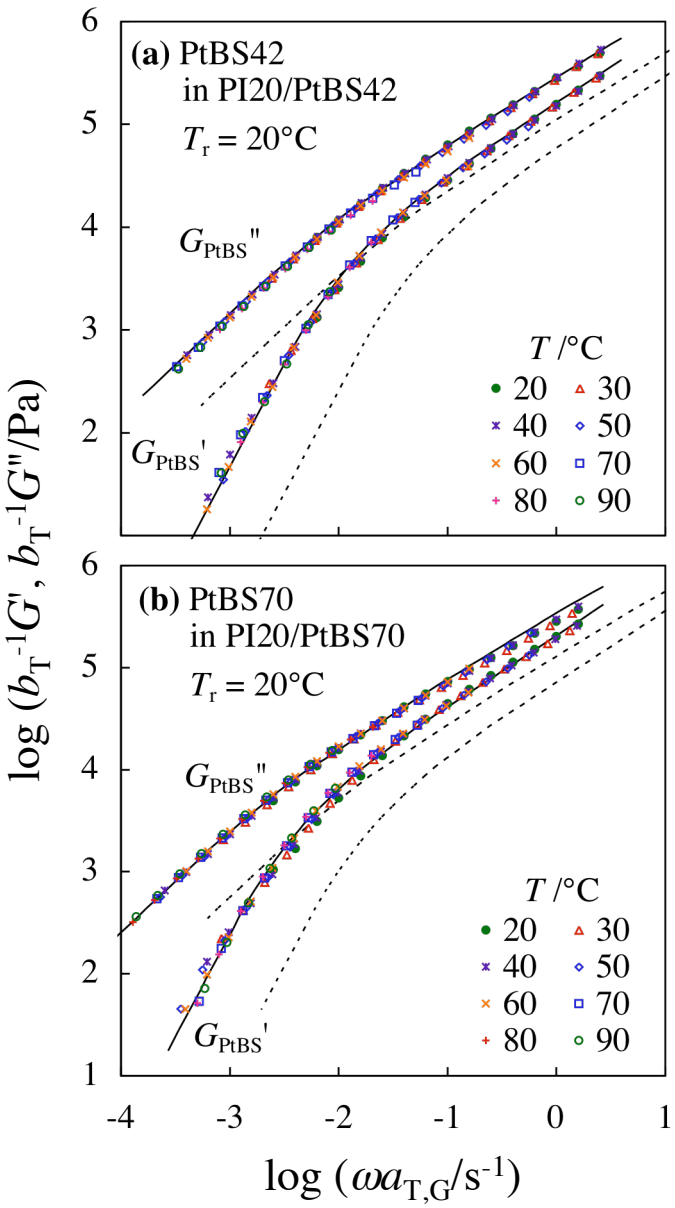
(a) PtBS42
in PI20/PtBS42
T_r = 20°C
G_{PtBS}"
G_{PtBS}'
T /°C
20 30
40 50
60 70
80 90
(b) PtBS70
in PI20/PtBS70
T_r = 20°C
G_{PtBS}"
G_{PtBS}'
T /°C
20 30
40 50
60 70
80 90
log ($b_T^{-1}G'$, $b_T^{-1}G''$/Pa)
log ($\omega a_{T,G}$/s^{-1})
6
5
4
3
2
1
-4
-3
-2
-1
0
1

Fig.8

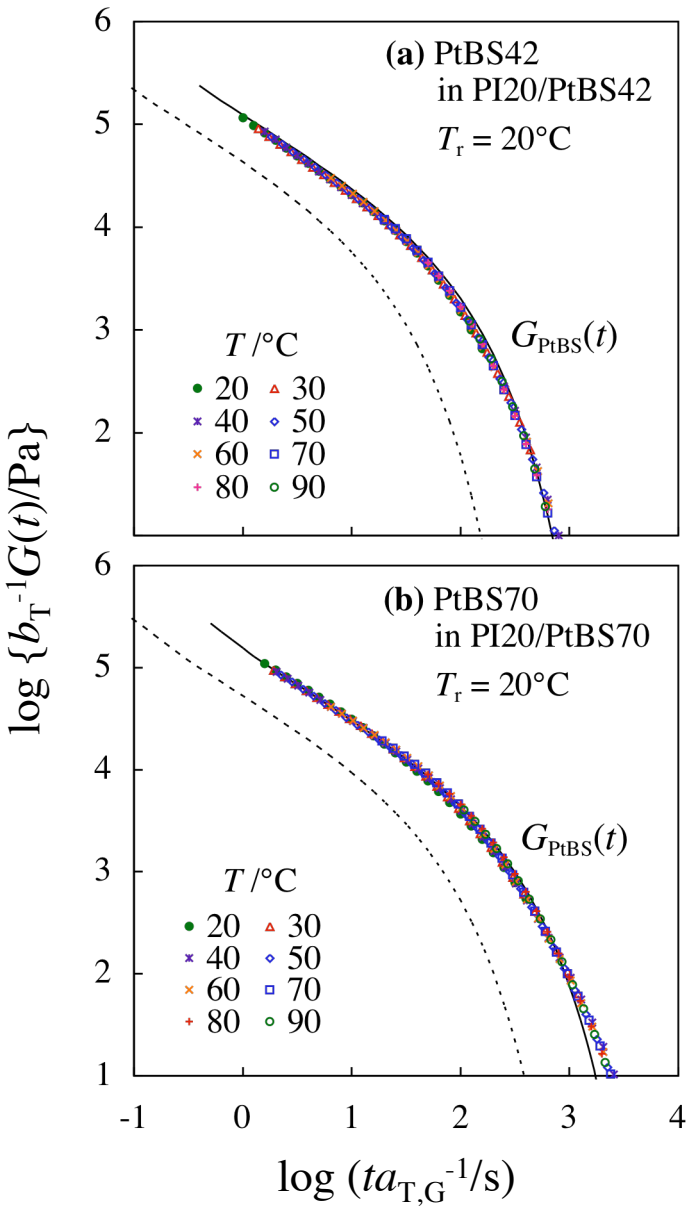
(a) PtBS42
in PI20/PtBS42
T_r = 20°C
$G_{PtBS}(t)$
T /°C
20 30
40 50
60 70
80 90
(b) PtBS70
in PI20/PtBS70
T_r = 20°C
$G_{PtBS}(t)$
T /°C
20 30
40 50
60 70
80 90
log {$b_T^{-1}G(t)$/Pa}
log ($ta_{T,G}^{-1}$/s)

Fig.9

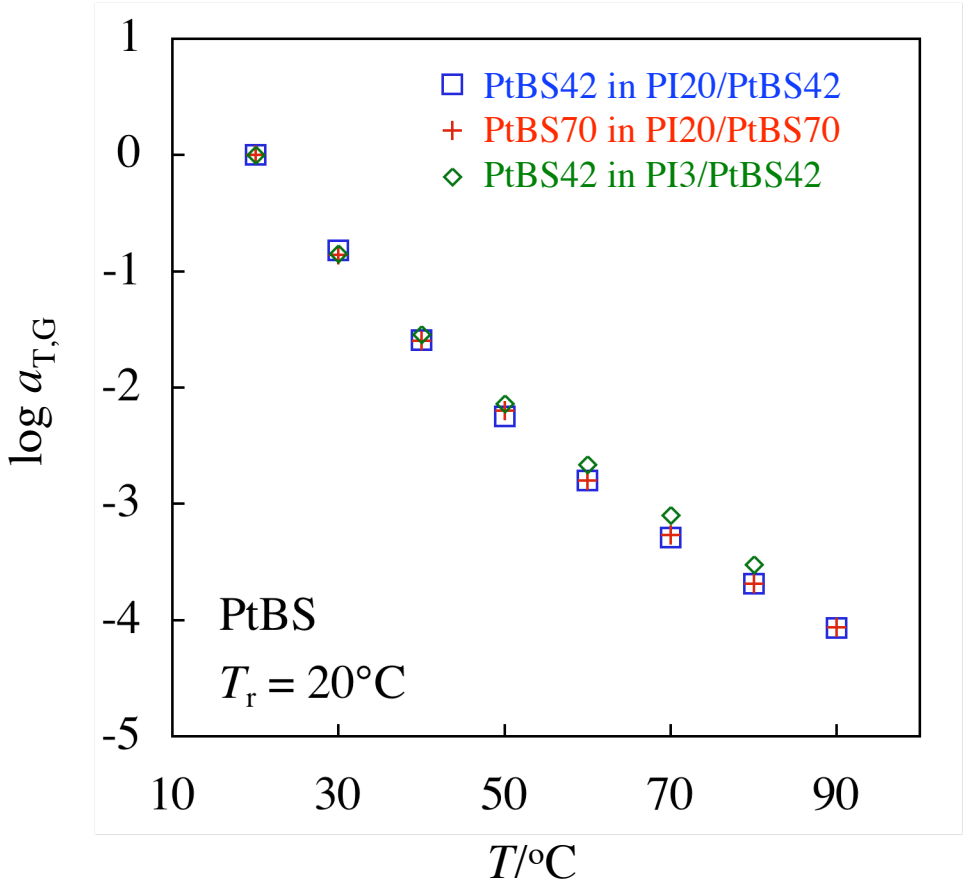
PtBS42 in PI20/PtBS42
PtBS70 in PI20/PtBS70
PtBS42 in PI3/PtBS42
PtBS
T_r = 20°C
log $a_{T,G}$
T/°C
1
0
-1
-2
-3
-4
-5
10
30
50
70
90

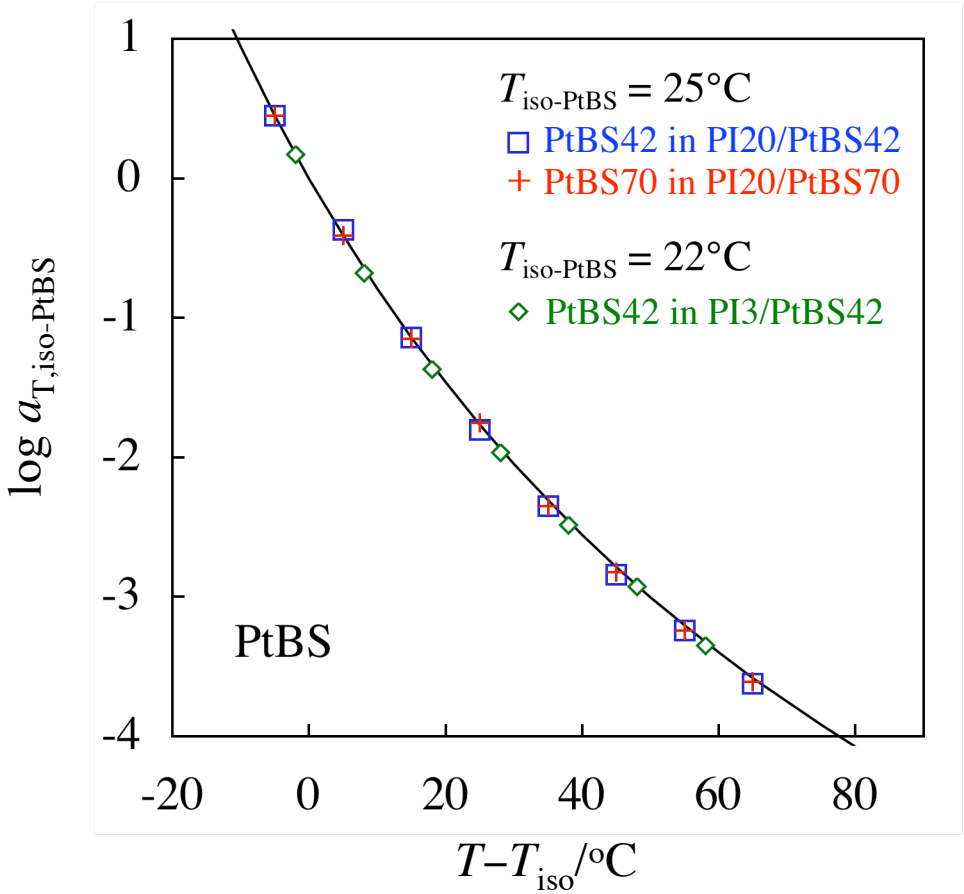
$T_{iso\text{-}PtBS}$ = 25°C
PtBS42 in PI20/PtBS42
PtBS70 in PI20/PtBS70
$T_{iso\text{-}PtBS}$ = 22°C
PtBS42 in PI3/PtBS42
PtBS
log $a_{T,iso\text{-}PtBS}$
$T-T_{iso}$/°C
1
0
-1
-2
-3
-4
-20
0
20
40
60
80

Fig.10

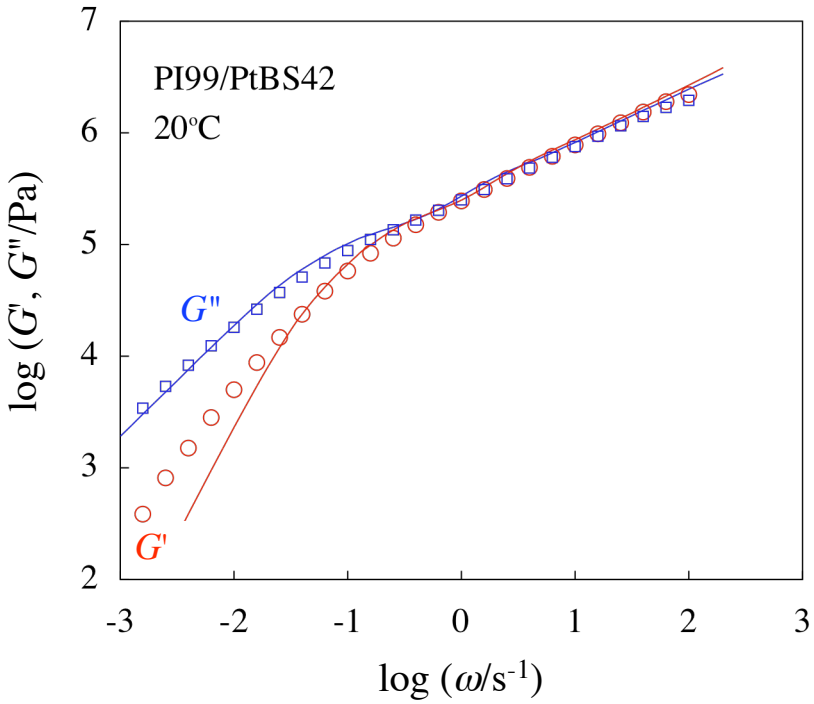

Fig.11

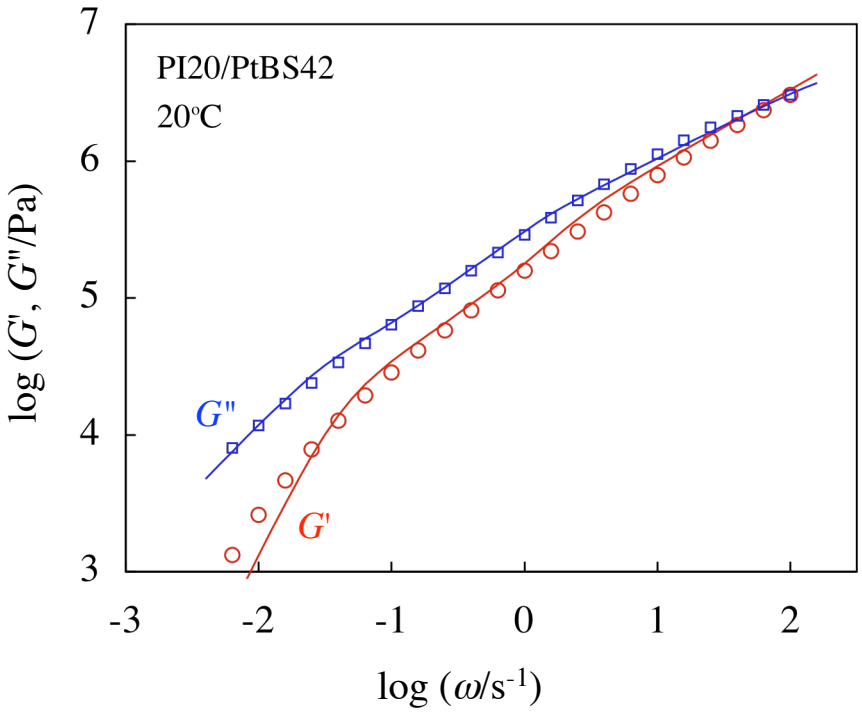

Fig.12

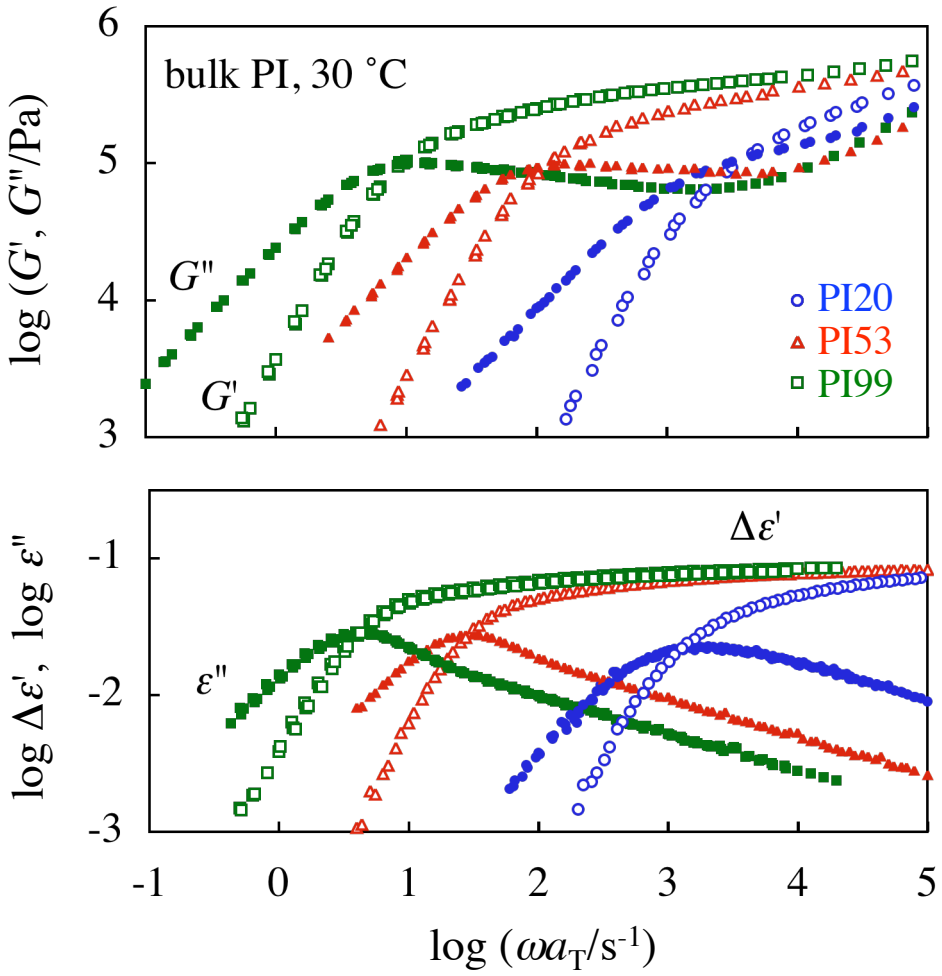
bulk PI, 30 ˚C
log (G', G"/Pa)
G"
G'
PI20
PI53
PI99
Δε'
ε"
log Δε', log ε"
log (ωa_T/s^-1)
6
5
4
3
-1
-2
-3
-1
0
1
2
3
4
5

Fig.13

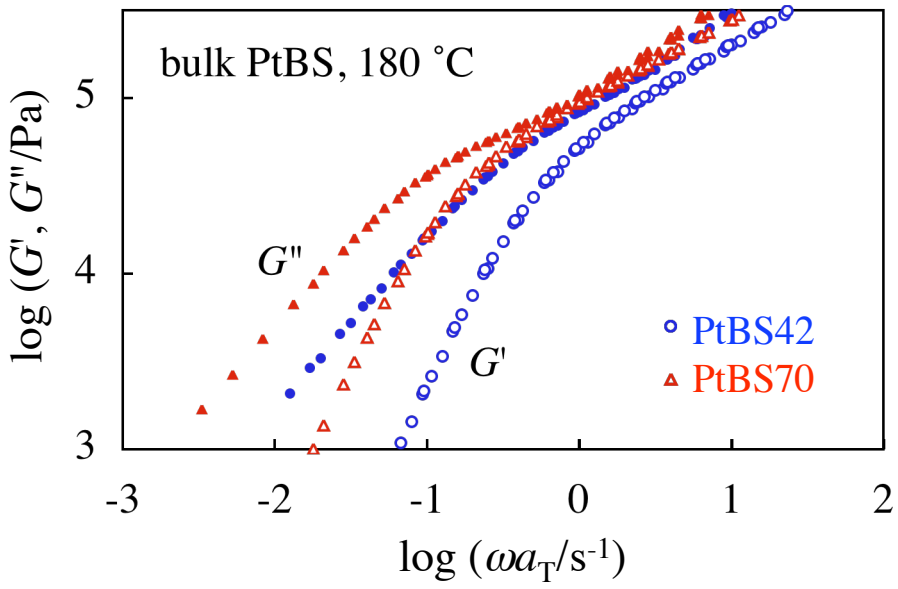
bulk PtBS, 180 ˚C
log (G', G"/Pa)
log (ωa_T/s^-1)
G"
G'
PtBS42
PtBS70
5
4
3
-3
-2
-1
0
1
2

Fig.14

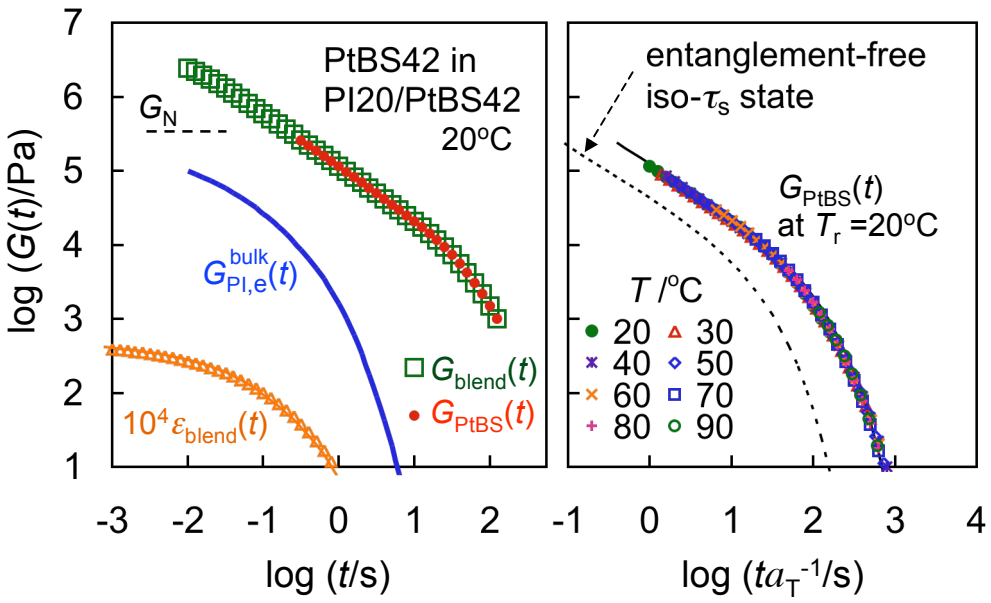
PtBS42 in
PI20/PtBS42
20°C
G_N
$G^{bulk}_{PI,e}(t)$
$G_{blend}(t)$
$G_{PtBS}(t)$
$10^4\varepsilon_{blend}(t)$
log ($G(t)$/Pa)
log (t/s)
entanglement-free
iso-τ_s state
$G_{PtBS}(t)$
at T_r =20°C
T /°C
20 30
40 50
60 70
80 90
log (ta_T^{-1}/s)

Fig.GA